→ THE ERS SAR WAVE MODE: A BREAKTHROUGH IN GLOBAL OCEAN WAVE OBSERVATIONS

The ERS SAR Wave Mode: A Breakthrough in Global Ocean Wave Observations

K. Hasselmann[1], B. Chapron[2], L. Aouf[3], F. Ardhuin[4], F. Collard[5], G. Engen[6], S. Hasselmann[7], P. Heimbach[8], P. Janssen[9], H. Johnsen[10], H. E. Krogstad[11], S. Lehner[12], J.-G. Li[13], X.-M. Li[14], W. Rosenthal[15], J. Schulz-Stellenfleth[16]

1 *Max Planck Institute of Meteorology, 20146 Hamburg, Germany. Klaus.Hasselmann@zmaw.de*
2 *IFREMER, 29280 Plouzané, France. bertrand.chapron@ifremer.fr*
3 *Météo-France, Division Marine et Océanographie, 31100 Toulouse, France. lotfi.aouf@meteo.fr*
4 *IFREMER, 29280 Plouzané, France. fabrice.ardhuin@ifremer.fr*
5 *OceanDataLab, 29280 Plouzané, France. dr.fab@oceandatalab.com*
6 *Norut, P.O. Box 6434, 9294 Tromsø, Norway. geir.engen@norut.no*
7 *Max Planck Institute of Meteorology, 20146 Hamburg, Germany. susanne.hasselmann@zmaw.de*
8 *Massachusetts Institute of Technology, Cambridge, MA 02139, USA. heimbach@mit.edu*
9 *ECMWF, Marine Aspects Section, Shinfield Park, Reading, RG2 9AX, UK. peter.janssen@ecmwf.int*
10 *Norut, PO Box 6434, 9294 Tromsø, Norway. harald.johnsen@norut.no*
11 *Norwegian University of Science and Technology, 7491 Trondheim, Norway. Harald.Krogstad@math.ntnu.no*
12 *German Aerospace Center (DLR), Remote Sensing Technology Institute, Oberpfaffenhofen, 82234 Wessling, Germany. Susanne.Lehner@dlr.de*
13 *Met Office, Exeter, Devon, EX1 3PB, UK. jian-guo.li@metoffice.gov.uk*
14 *German Aerospace Center (DLR), Remote Sensing Technology Institute, Oberpfaffenhofen, 82234 Wessling, Germany. Xiao.Li@dlr.de*
15 *Helmholtz-Zentrum Geesthacht, 21502 Geesthacht, Germany. wolfgang.rosenthal@hzg.de*
16 *Helmholtz-Zentrum Geesthacht, 21502 Geesthacht, Germany. Johannes.Schulz-Stellenfleth@hzg.de*

1. Introduction

The first European Remote Sensing satellite, ERS-1, launched on 17 August 1991, was conceived in the 1980s, at a time of growing scientific and public awareness of the need to better understand, monitor and manage the Earth system. The dangers of environmental degradation, the alarming increase in the rate of loss of species, and the threat of irreversible climate change had emphasised the need to treat Earth as an integrated system. Satellites provided a unique opportunity to obtain the necessary global, continuous datasets. And an ocean satellite would clearly be needed as a key component of an integrated satellite Earth observation system in order to monitor the oceans, which cover more than two-thirds of Earth's surface, and the ocean–atmosphere interface.

To achieve a 24-hour, all-weather global capability, it was decided that the main instrument on ERS-1 would be a multi-component Active Microwave Instrument (AMI), consisting of a scatterometer, a radar altimeter and a Synthetic Aperture Radar (SAR). Since they can see through clouds and are independent of sunlight, microwave systems have the great advantage of being able to operate under all conditions. The proof of concept of satellite-based microwave measurements of the ocean had been provided by the NASA–NOAA satellite Seasat, launched in August 1978. Although Seasat unfortunately failed through a power short-circuit after only 100 days of operation, initial analyses had demonstrated that microwaves, reflected or backscattered from the sea

surface, could provide valuable data on sea surface heights, sea surface winds, wave heights and many other important features.

In particular, it had been shown that the SAR could reveal detailed structural information on a wide variety of ocean phenomena. The SAR is an advanced radar imaging instrument that achieves high resolution not only in the range direction, through the standard radar technique of measuring the travel time of short microwave pulses, but also in the along-track (azimuthal) direction, by exploiting the Doppler shift induced by the satellite motion. The achievable azimuthal resolution is then of the order of the antenna length, as opposed to the inverse dependency on the antenna length for a conventional radar. The ocean surface features imaged by the Seasat radar included the propagation directions and wavelengths of surface waves and internal waves, current-induced surface signatures of bottom topography, and the distribution of oil slicks, eddies and fronts.

Seasat not only provided a major technical impetus for an improved follow-on European satellite ERS-1, but also created a strong motivation for European scientists to engage in satellite remote sensing of the oceans. The collaboration with American colleagues had demonstrated to European scientists the exciting opportunities that all-weather global satellite measurements offered for studies of the ocean, the coupled ocean–atmosphere system and the cryosphere. Particularly influential in this respect was John Apel (1930–2001), a long-standing advocate of ocean remote sensing and a key player in the Seasat project.

One of the many important applications of ERS-1 (1991–2000) and its successors ERS-2 (1995–2011) and Envisat (2002–12) was in the field of ocean waves. The launch of ERS-1 came at an opportune time for ocean wave research. In the three decades prior to the launch of ERS-1, detailed theoretical studies and extensive field programmes had led to major advances in our understanding of the dynamics and propagation of wind-driven ocean waves. Numerical wave models, such as the WAM model (WAMDI, 1988), had been developed to compute the space–time evolution of the two-dimensional ocean wave spectrum, for given wind field forcing, as a function of period and propagation direction (for a comprehensive summary of ocean wave research and modelling, see Komen et al., 1994). What were needed now to drive the models were good surface wind data, and, to initialise and validate the models, good wave data. The combined modes of the Active Microwave Instrument of ERS-1 were able, in principle, to provide all the data needed: surface winds, from the scatterometer and Radar Altimeter; mean wave heights, also from the Radar Altimeter; and the full two-dimensional surface wave spectrum, from the SAR.

2. The SAR Wave Mode

The SAR, as the most sophisticated of the AMI systems, provided potentially the most detailed ocean wave information. To reduce the so-called clutter noise, four single-look SAR images, with a theoretical resolution of 4 m, were averaged to produce multi-look images of about 20 × 16 m resolution. The SAR instrument produced millions of images of the ocean surface at this extremely high spatial resolution. But it also presented two major challenges: achieving global coverage and retrieving calibrated two-dimensional ocean wave spectra from the SAR images.

The difficulty in achieving global coverage was that, in continuous operation, the available data generation rate of the SAR was far too large for onboard storage of the data and later transmission to a ground receiving station, after the satellite came in sight of one of the relatively few ground stations. The problem was resolved by introducing two operating modes for the SAR: a standard broad-swath mode, which could be switched on when

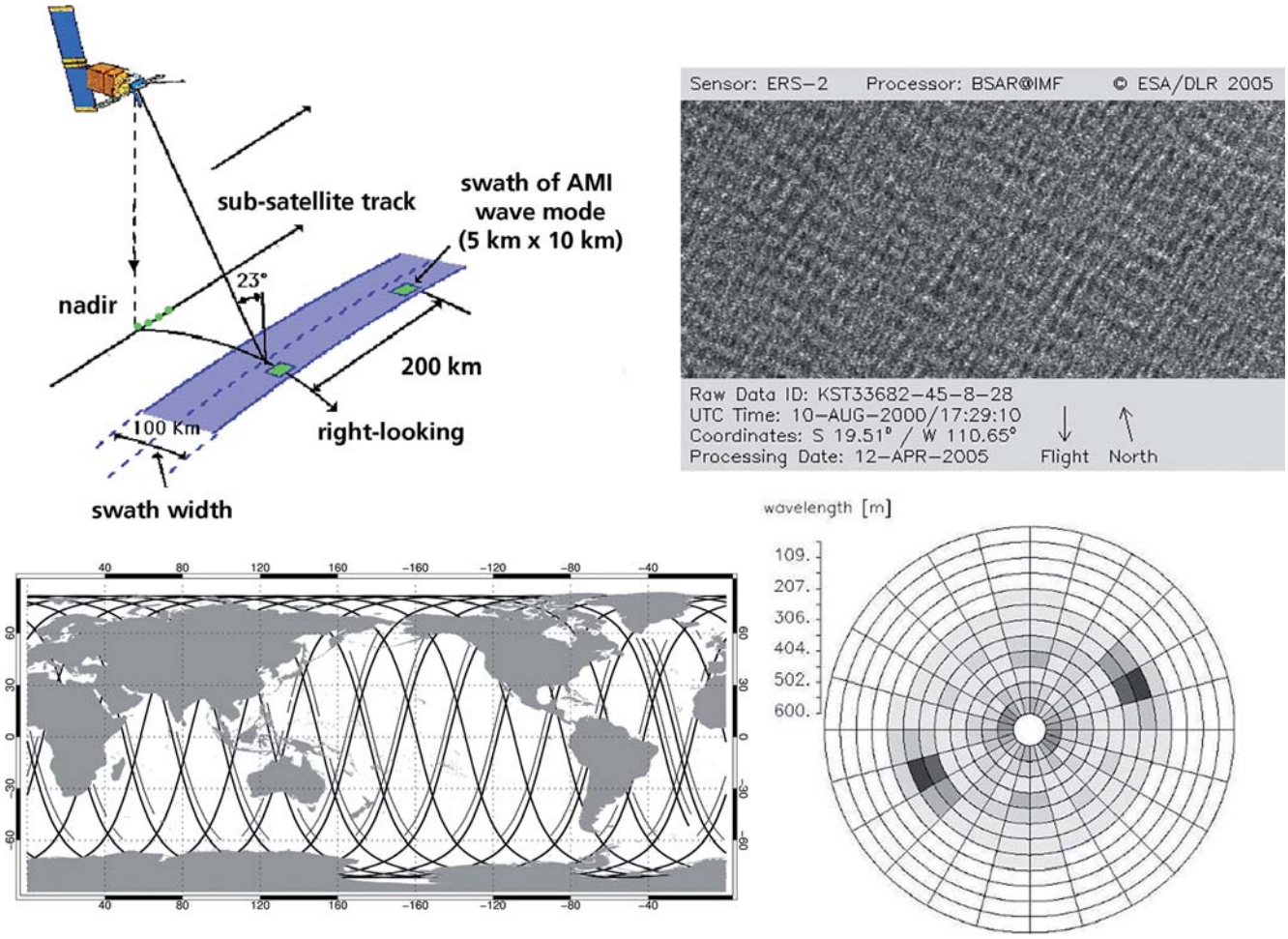

Figure 1. ERS-1 orbits and footprints of the nadir-looking Radar Altimeter and the full-swath SAR of the AMI. The wave-mode SAR was switched on briefly every 200 km along the satellite track, producing a 5 × 10 km SAR imagette (*top right*). (From Lehner et al., 2000; DLR) *Bottom right:* Example of the standard SAR wave mode product delivered by ESA. (Brooker, 1995)

the satellite was in sight of a ground station, to which the SAR data could then be transmitted directly, and a global SAR wave mode, designed with a periodic on/off operation cycle. The SAR wave mode was activated only for a short period every 200 km along the orbit, producing 5 × 10 km rectangular 'imagettes' (see Fig. 1, top right). (In Envisat, which succeeded ERS-1/ERS-2, the separation between imagettes was reduced to 100 km).

The wave mode data were sufficiently reduced relative to the full-swath data that they could be stored aboard the satellite until the data could be transmitted to a ground station in sight of the satellite. Although small, the imagettes, were nevertheless sufficiently large compared with the wavelengths of ocean waves to retrieve a meaningful statistical ocean wave spectrum. They were also sufficiently closely spaced to be compatible with the spatial resolution of current numerical global ocean wave prediction models, as applied, for example, in the daily global wave forecasts of the European Centre for Medium Range Weather Forecasts (ECMWF).

The SAR wave mode imagettes were obtained at a mean incidence angle of 23°, within the low-incidence-angle region of the broader scatterometer swath (see Kerbaol et al., 1998, for a detailed description and analysis). Together with the Radar Altimeter wave heights measured directly below the satellite orbit and the winds retrieved from the scatterometer, these data provided a valuable and unique synergistic dataset that could be used both as inputs to numerical wave prediction models and as data for model validation.

The second basic problem in the SAR imaging of ocean waves was the interpretation of the images. Seasat had clearly demonstrated that the SAR could see ocean waves (see Johannessen et al., this volume, for similar full-swath examples for ERS). But what was the relation between the waves seen in the image and the real waves in the ocean? Since the standard SAR image processing assumed that the Doppler was produced only by the satellite motion, the imaging theory could not be directly applied to random time-varying surfaces such as the sea surface. In particular, doubts had been expressed that SAR images could be used for quantitative measurements of ocean waves due to the orbital motions of the long waves that transport the short Bragg waves (in the 20 cm wavelength range) responsible for the microwave backscatter. The additional Doppler shift induced by the long-wave orbital velocities leads to a misplacement of the inferred position of the backscattered surface element, resulting in a distortion of the inferred wave spectrum. In one of the first analyses of these effects, Alpers & Rufenach (1979) pointed out that, depending on the wave steepness and propagation directions, some wave components would thereby be enhanced, while others would be smeared out.

A first convincing demonstration that, despite these concerns, SAR wave image data could nevertheless provide useful information on wave spectra was provided by the analysis of the full wave dataset from a Seasat orbit (Fig. 2, left). The inferred centre of high winds that produced the swell agreed well with the wind field reconstructed from weather data (Fig. 2, right).

Yet this successful reconstruction of the swell sources from SAR wave data glossed over some of difficulties emphasised by Alpers & Rufenach (1979). Since the Seasat SAR wave data were uncalibrated, only the wavelengths and propagation directions of the wave retrievals were used, not the wave amplitudes. Moreover, the swell fields were well dispersed, corresponding to

Figure 2. *Left:* Principal propagation directions of swell derived from the SAR wave images of the SEASAT orbit 757, acquired at 22:47 UTC on 18 August 1978, with the position of the inferred extratropical cyclone. (From Lehner, 1984) *Right:* Contour plot of surface wave heights (in metres) derived from a later reanalysis of the ECMWF data (ERA-40) at 18:00 UTC on 17 August 1978.

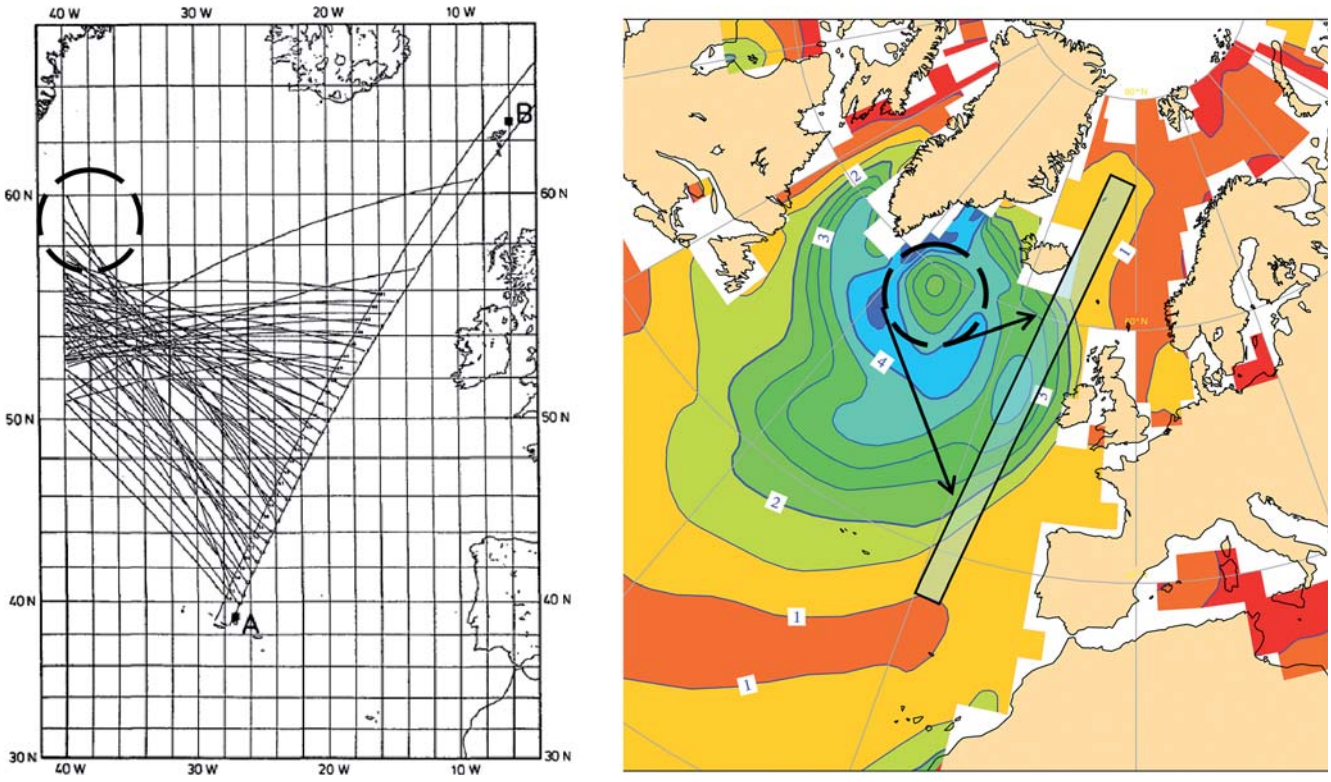

narrow directional spectra. In this case, the different weightings assigned by the SAR to different propagation directions produced no significant distortions. Finally, the long swell waves were propagating in the near-range direction (i.e. orthogonal to the satellite flight direction) and had low steepness. In this case, the distortions induced by the wave orbital motions were small and, if anything, enhanced the imaging.

ERS SAR data are now widely used to track waves emanating from storm regions, using both the SAR wave mode and full-swath data (see below). The SAR enables the routine reconstruction of the high-wind source region of the swell and decay rates of the swell as it propagates over many thousands of kilometres, using the basic spectral wave propagation relations first applied by Barber & Ursell (1948) to infer the locations and times of the distant storms that produced the swell. The SAR wave retrieval methods have meanwhile become more sophisticated, yielding well calibrated wave spectra. However, care must still be taken to allow for the distortions induced by the nonlinearity of the imaging mechanism, as discussed in the next section.

3. Retrieval of Ocean Wave Spectra from SAR Images

In anticipation of the difficulties of retrieving quantitative wave spectral data from SAR images not only in individual case studies, but also for the more general application of operational wave prediction, an extensive field programme, the Marine Remote Sensing Experiment (MARSEN), was carried out in 1979. The experiment, involving numerous research aircraft, ships, wave measurement stations, etc., from Europe and the US, was originally planned as a Seasat underflight project. However, when Seasat failed in 1978, it was rescheduled as a field programme in support of the planned European successor to Seasat.

MARSEN yielded invaluable insights. Among other results, it led to an extensive multi-author collective analysis of the theory of the SAR imaging of ocean waves (Hasselmann et al., 1985). This provided the basis for the design of the ERS-1 SAR wave mode instrument and the later retrieval of ocean wave spectra from the wave mode imagettes.

Figure 3 illustrates the impact of velocity bunching on the SAR imaging of ocean waves. For a small azimuthal component of the wave steepness, the velocity bunching can be represented by a linear transfer function. This can be simply added to the two other linear transfer functions characterising the radar imaging of ocean waves: the hydrodynamic and tilt modulation of the short backscattering Bragg waves (in the centimetre range) by the imaged long ocean waves (in the range 10–1000 m). The hydrodynamic and tilt transfer functions apply equally to real and synthetic aperture radars and are reasonably well understood. However, the velocity bunching mechanism rapidly becomes nonlinear when the wave steepness increases and the displacement direction, which is in the satellite flight direction, is parallel to the propagation direction of the waves. When these two effects are superimposed, in particular for short steep waves travelling parallel to the flight (azimuthal) direction, the wave image can become completely smeared out (see lower part of Fig. 3).

Thus, in order to retrieve quantitative ocean wave spectra from SAR image spectra, two developments were necessary: a theory of the nonlinear mapping of an ocean wave spectrum into a SAR image spectrum, and a method for inverting the nonlinear mapping relation to infer the wave spectrum from the measured SAR wave spectrum. Both problems were successfully solved, the first rigorously, the second more approximately, leading to different inversion schemes (Hasselmann & Hasselmann, 1991; Krogstad et al., 1994; Engen et al., 1994; Hasselmann et al., 1996; Mastenbroek & de Valk, 2000; Chapron et al., 2001; Schulz-Stellenfleth et al., 2005; Collard et al., 2009).

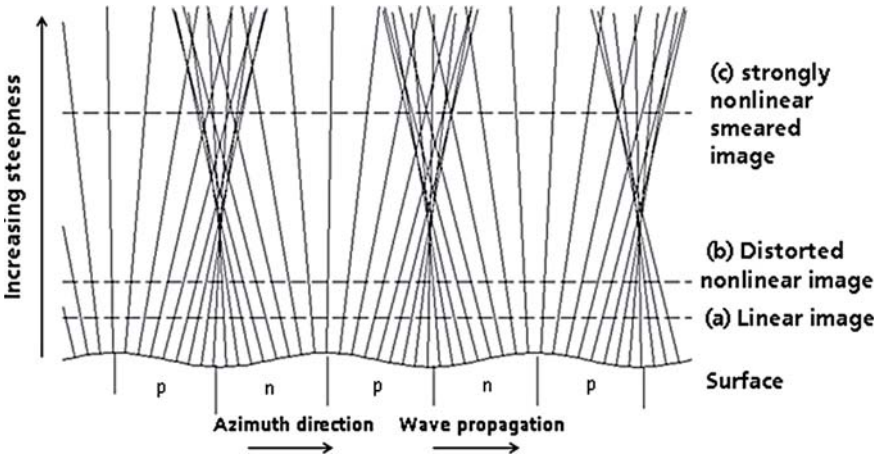

Figure 3. Velocity bunching: Impact of wave orbital motions on the SAR-imaged position of a backscattering surface element of a wave field. The vertical axis refers to the average wave steepness. For a given steepness, the imaged position of an element on the sea surface is given by the intersection of the associated ray with the horizontal line corresponding to the given wave steepness. p and n indicate the orbital motions of water particles toward and away from the SAR platform. (Courtesy of X.-M. Li, after Hasselmann et al., 1985)

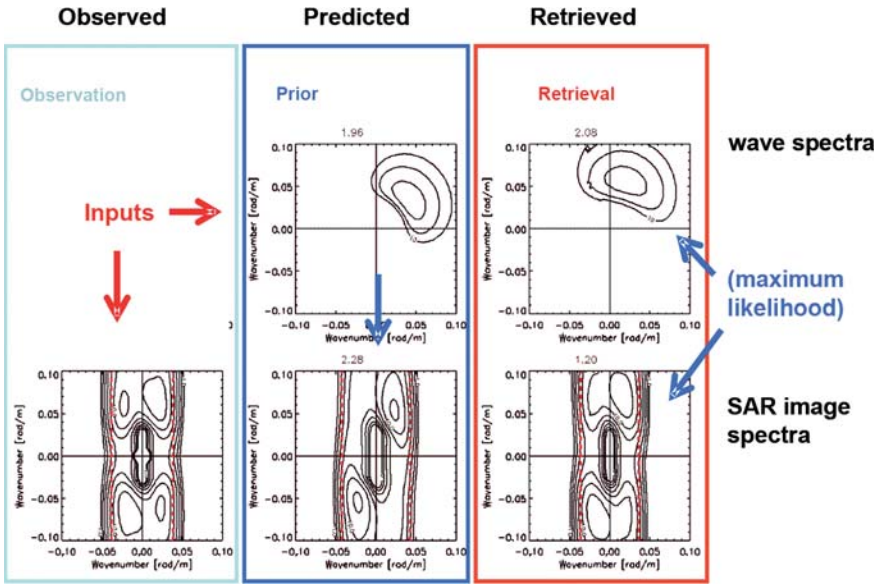

Figure 4. Contour plots of observed and computed 2D wavenumber spectra.

The original inversion method of Hasselmann & Hasselmann (1991) is illustrated in Fig. 4. It is based on a maximum likelihood matching of the first-guess (prior) information available from a wave model and the data provided by the SAR wave image spectrum. From the first-guess wave spectrum, the forward transform is applied first to compute the associated SAR wave image spectrum. This will generally differ from the observed SAR wave image spectrum. One then constructs a maximum likelihood resultant wave spectrum and an associated SAR wave image spectrum by linearly combining the two (generally inconsistent) sets of information. The final maximum likelihood (posterior) wave spectrum depends on the weights assigned to the two separate sets of information. It is then possible to effectively disregard the regions of the SAR image spectrum in which the wave components are strongly distorted by the velocity bunching mechanism, the unreliable information being replaced by the predicted first-guess spectrum. The method necessarily depends on the subjective assessment of the reliability of the first-guess wave spectrum, which is derived from integrated information on winds and waves over a larger area around the location of the retrieval, compared with the reliability of the SAR wave spectral image (which may well have problems apart from the distortions induced by velocity bunching).

The first generation of retrieval algorithms yielded a wave spectrum corresponding to a frozen image of the sea surface. They were thus unable to resolve the 180° directional ambiguity of the wave propagation directions of

a frozen image without additional information, such as from the first-guess wave model prediction. However, the required information was, in principle, available in the multi-look SAR data itself. Instead of simply averaging four successive looks (in order to reduce the clutter noise), it was possible to determine small changes between successive looks due to the propagation of the waves. Technically, the directional ambiguity was removed by computing not only the spectrum for the averaged looks, but also the complex cross-spectrum between successive looks (Vachon & Raney, 1991; Vachon & West; 1992). The analytic nonlinear ocean SAR transform based on cross-spectra and the corresponding inversion was published by Engen & Johnsen (1995). Following a proof-of-concept using reanalysed ERS-2 data, cross-spectra were incorporated in the standard ESA SAR wave mode product for the following satellite Envisat (Johnsen et al., 1998; Lehner et al., 2000).

The original maximum-likelihood method of Hasselmann & Hasselmann (1991) (Fig. 4) was generalised accordingly, such as by ECMWF (Abdalla et al., 2004) and in the PARSA retrieval algorithm of Schulz-Stellenfleth et al. (2005), to derive two-dimensional wave spectra free from directional ambiguities.

The need to augment SAR wave image data using independent wave data from other sources – preferably from a state-of-the-art wave model used for operational global wave prediction – nevertheless remains an inherent limitation of SAR wave spectral data in all cases in which the azimuthal spectral cutoff due to velocity bunching cannot be neglected. Attempts to circumvent this limitation have used two approaches.

The first approach is simply to limit the retrieval at the outset to the spectral range not seriously affected by the azimuthal cutoff. There exists a broad range of interesting problems, in particular regarding the propagation of swell (as illustrated in Fig. 2 and further examples discussed below), for which this approximation is quite acceptable. The second approach is to substitute the detailed spectral information provided by a state-of-the-art wave spectral model by auxiliary information obtained, for example, from scatterometer-derived surface winds or Radar Altimeter wave heights. This leads to the difficulty, however, that the missing azimuthal cutoff data are of a specific spectral structure, whereas the substitute data necessarily represent spectral integrals that are unable to resolve the missing spectral information.

Thus, in summary, the various proposed SAR wave spectrum retrieval algorithms can be classified with respect to two characteristics. First, whether they are first-generation retrievals ('1'), based only on the standard image variance spectrum, or second-generation retrievals ('2'), using inter-look cross-spectral data. Second, whether they use state-of-the-art wave model predictions as first-guess input data (M), are limited to swell-type spectral data (S), in which the spectral components affected by the azimuthal cutoff can be neglected, or, finally, use auxiliary data instead of a first-guess model to augment the spectral region affected by the cutoff (A). An example of retrieval type 1S is the swell study of Lehner presented in Fig. 2; examples of the application of the other retrieval types will be discussed in subsequent sections.

Parallel to these different development strands, all retrieval algorithms have benefited from continuous technical improvements. These include improved formulations of the imaging transfer functions, special retrieval algorithms for selected integrated spectral properties, analysis of image pixel statistics, and investigations of the signal-to-noise and image contrast problems associated with the inter-look cross-spectral analysis method used to remove the directional ambiguity (Schulz-Stellenfleth et al., 2005).

4. Comparison of Retrieved SAR Wave Spectra with Operational Wave Model Predictions

A comprehensive comparison of three years of ocean wave image spectra retrieved from ERS-1 SAR with the wave spectra predicted by the ECMWF operational global wave model was undertaken by Heimbach et al. (1998); see Fig. 5. This provided the first quantitative assessment of the quality of the ECMWF wave forecasts over a continuous period, covering all seasons and on a global scale. A similar study on a regional scale, using the Norwegian operational wave prediction model, was undertaken by Breivik et al. (1998). In both studies a type 1M retrieval algorithm was applied.

The availability of a first-guess wave field was important for the retrieval of the wind sea spectrum (Fig. 5, left panels), but not critical for the swell components (right panels), which consisted largely of well dispersed wave systems, in which the velocity bunching could be linearised. The retrieval algorithm was upgraded in this analysis by subdividing the wave spectrum into a number of separate wave systems, which were then inverted individually (Hasselmann et al., 1996). In a complementary study, Bauer & Heimbach (1999) compared SAR-retrieved significant wave heights (using the same retrieval algorithm) against those obtained independently from the altimeters on ERS-1 and Topex/Poseidon. As in

Figure 5. Seasonally and ocean-basin averaged polar diagrams of wave heights and directions (defined analogously to the standard wind vector polar diagrams of operational meteorology). *Left:* Wind sea spectra. *Right:* swell. Solid lines: ERS-1 SAR wave mode data; dashed lines: ECMWF-WAM model predictions. (From Heimbach et al., 1998)

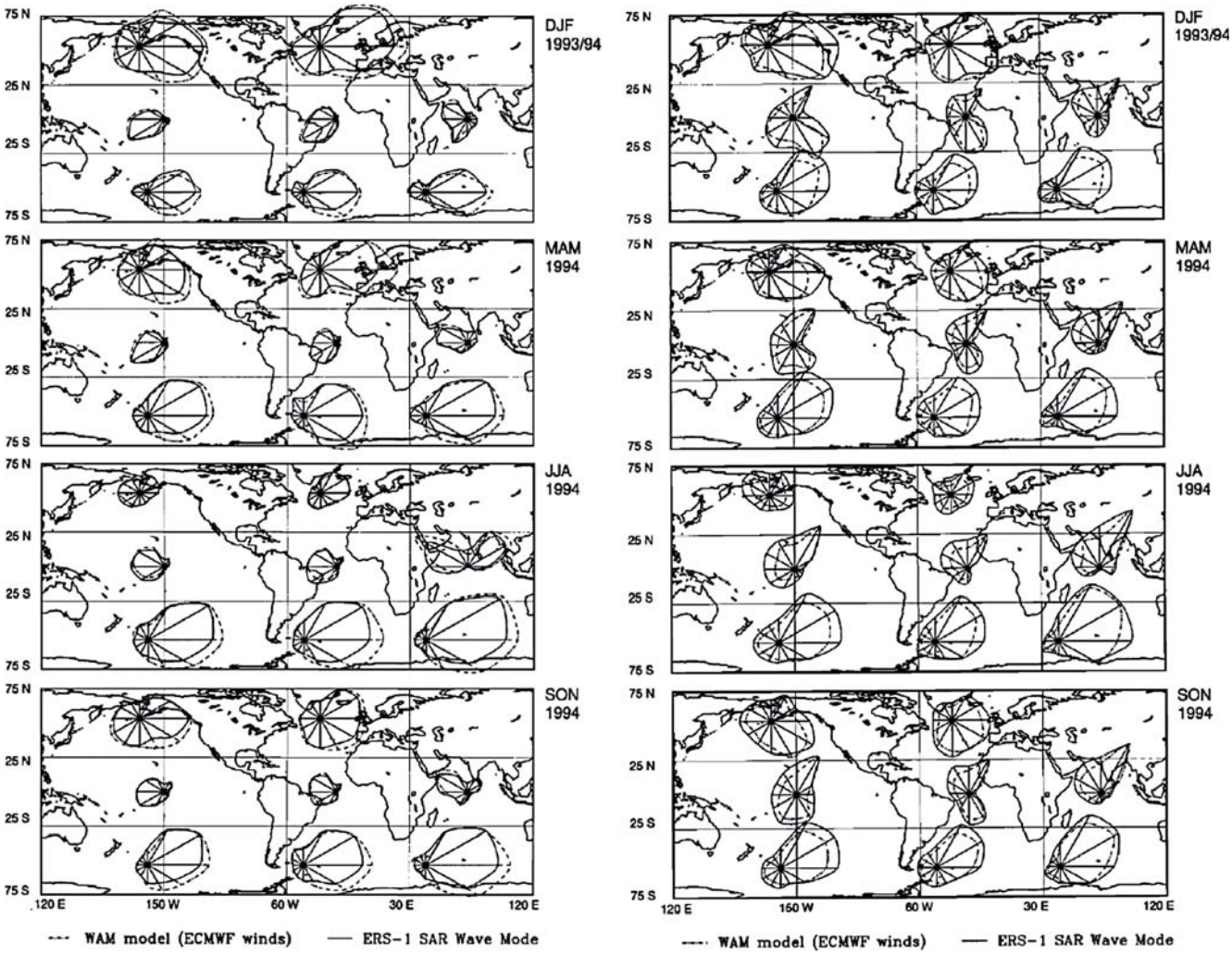

other applications of type 1M retrieval algorithms using first-guess wave spectra from a wave model, the directional ambiguity presented no serious limitation, as this could be resolved by the first-guess data from the wave model.

The overall agreement between the SAR-retrieved and predicted wave data as well as with independent wave measurements was clearly very encouraging. At this stage, no attempt had been made to assimilate the retrieved SAR wave data in the wave model. Thus, the investigation was a test of the mutual consistency of the wave model prediction, driven by winds produced by the standard ECMWF weather analysis, and the wave spectra retrieved from the SAR. Despite the good overall agreement, systematic seasonally and regionally dependent deviations between the model and retrieved polar wave height diagrams are clearly visible. At that time, a tendency was revealed for the ECMWF model to predict too high wind seas and too low swell, indicating that both the wind input and the swell dissipation source terms in the wave model needed to be modified. This has led to successive improvements in the wave model.

With the later model updates and the assimilation of SAR wave spectral data and Radar Altimeter wave heights, the ECMWF operational wave prediction model has now reached a level of maturity (see Figs 6–9) that the current

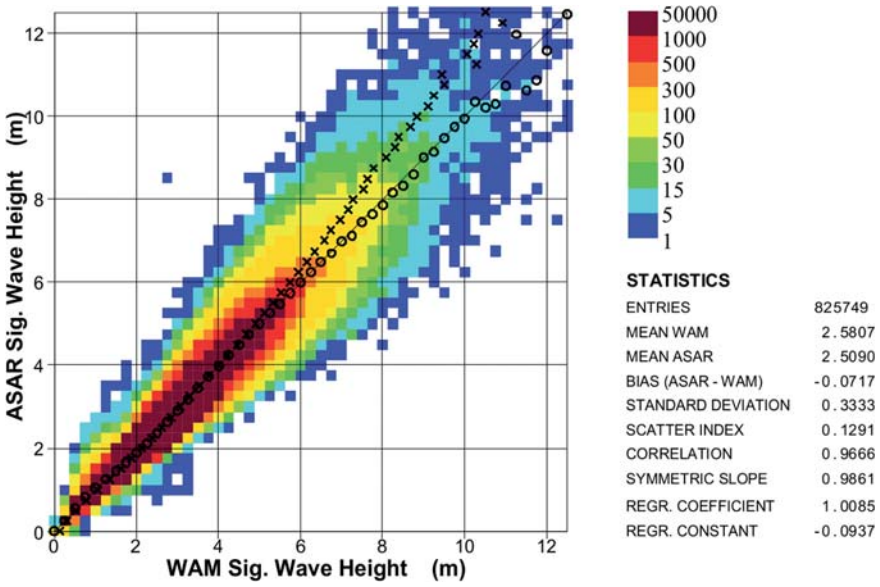

Figure 6. Global comparison of inverted Envisat/ASAR Level 1b data and WAM model results for significant wave heights, 2009 (Abdalla et al., 2010). (Peter Janssen, ECMWF)

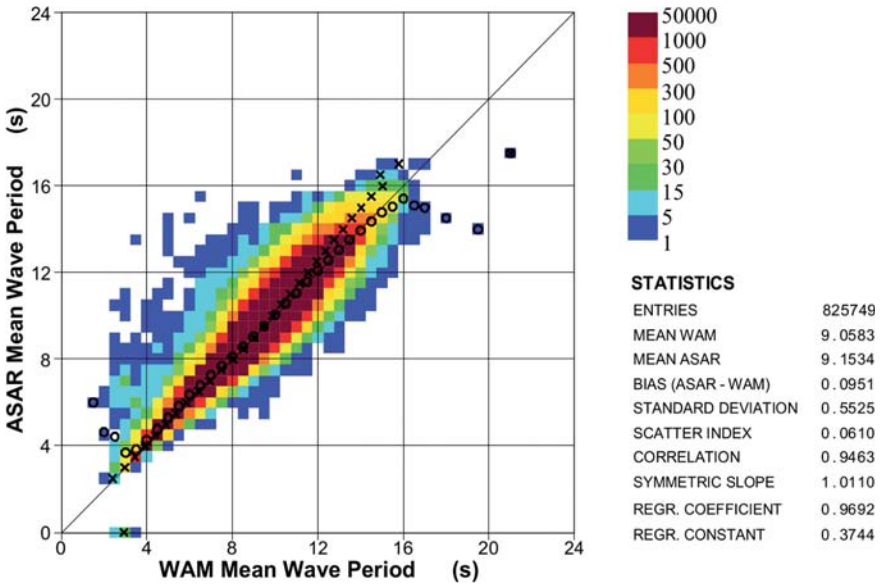

Figure 7. Global comparison of inverted Envisat/ASAR Level 1b data and WAM model results for mean wave period, 2009 (Abdalla et al., 2010). (Peter Janssen, ECMWF)

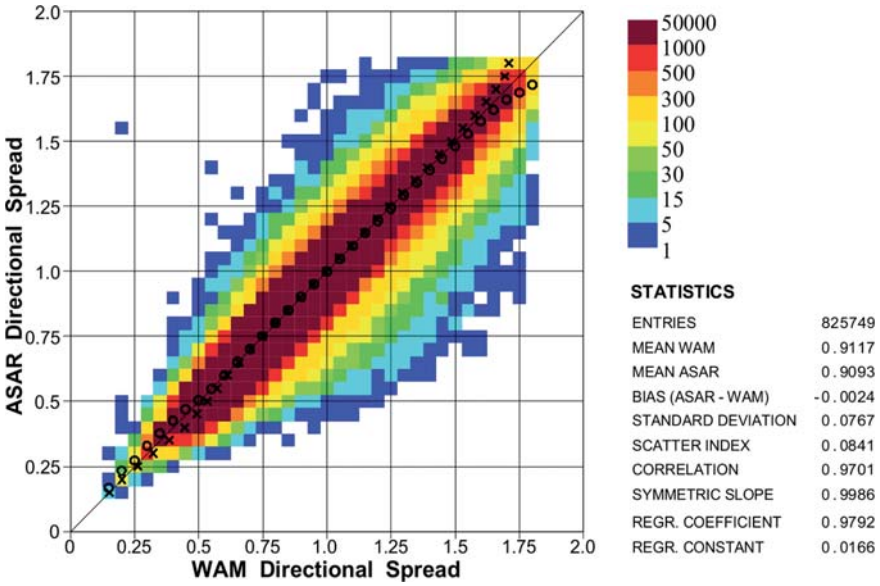

Figure 8. Global comparison of inverted Envisat/ASAR Level 1b data and WAM model results for mean directional spread, 2009 (Abdalla et al., 2010). (Peter Janssen, ECMWF)

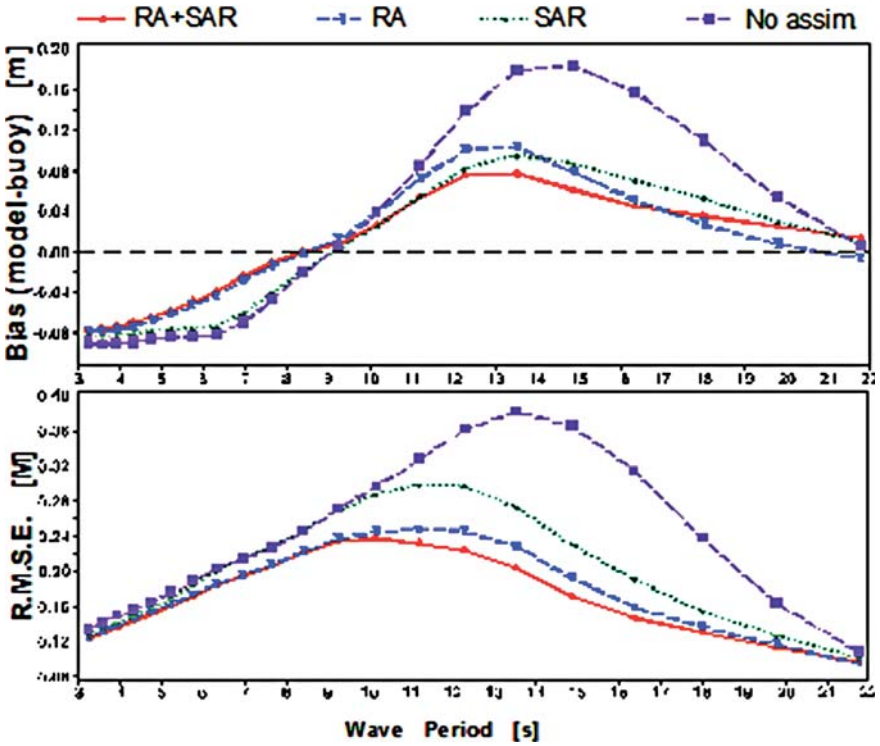

Figure 9. Impact of various assimilation setups (ERS-2 RA and SAR) on the bias and rms error of a one-dimensional wave spectrum, verified against *in-situ* buoy observations, 1–29 May 2001. (Abdalla et al., 2004)

operational SAR wave data assimilation scheme has only a minor impact on the skill of the prediction (Fig. 9). However, this level of maturity could not have been reached without the two-dimensional wave spectra provided as verification data by the global SAR wave mode system.

The above comparisons of retrieved and predicted wave spectra were still based on a first-generation type 1M retrieval algorithm, in which the directional ambiguity of the SAR image spectra had not been removed. Figures 10 and 11 show similar comparisons using the type 2M PARSA retrieval algorithm. Figure 10 illustrates that in this case it is meaningful to compare not only the directional spread (as in Fig. 8), but also the mean direction itself. The impact of combining model and retrieved fields in the simultaneous determination of both the retrieved and predicted wave spectra is illustrated in Fig. 11, which shows comparisons of retrieved and predicted wave heights for two models,

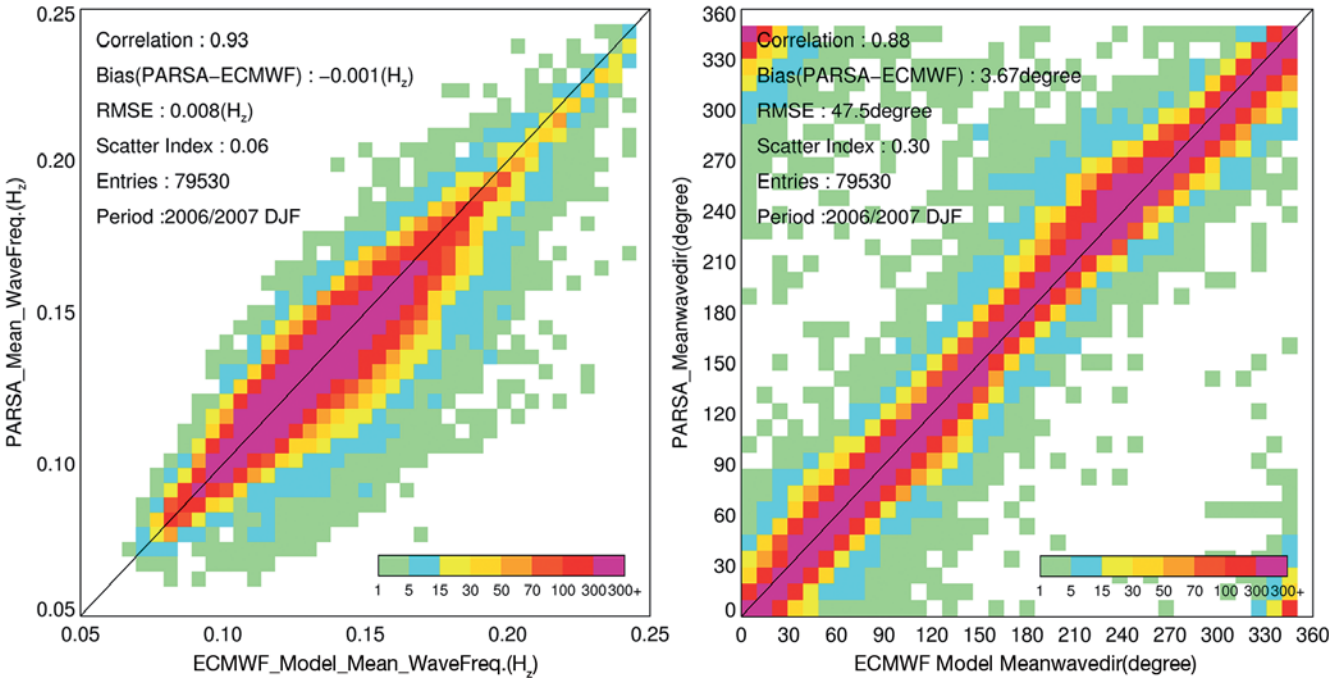

Figure 10. Comparisons of the PARSA mean frequency (*left*) and mean wave direction (*right*) with those of the ECMWF reanalysis wave model. (Li et al., 2010)

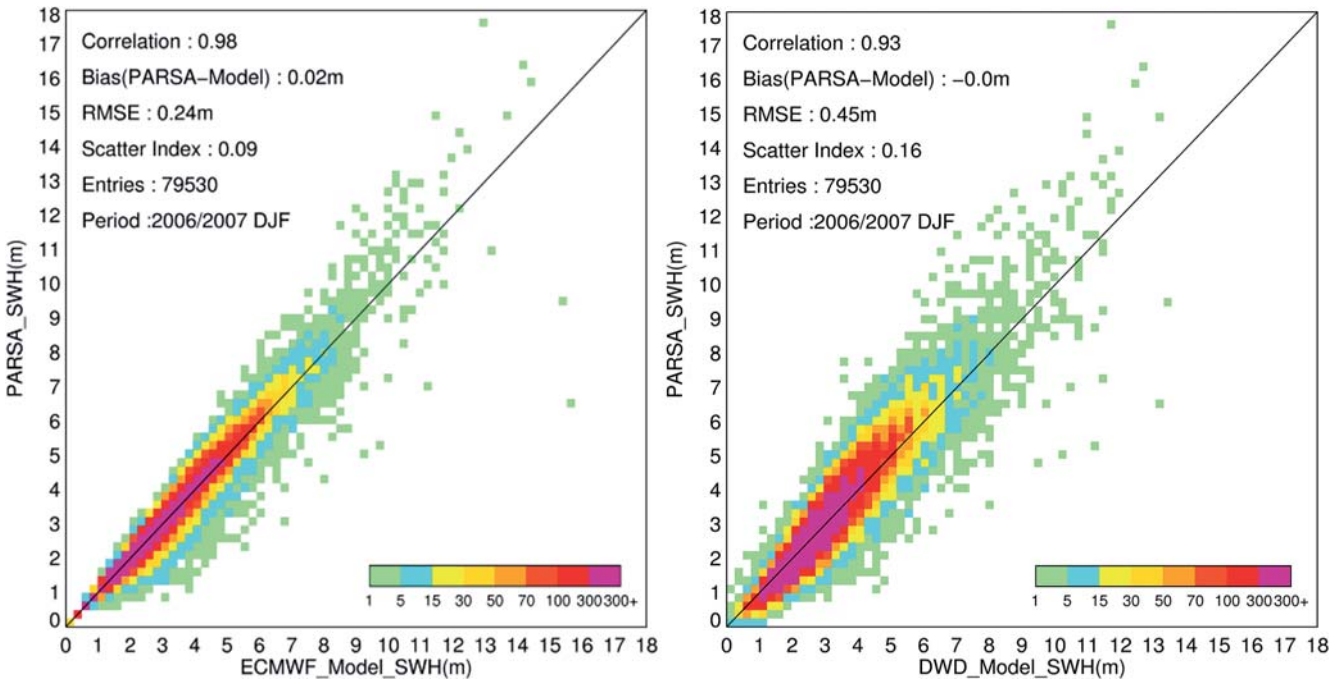

Figure 11. Comparisons of the PARSA significant wave heights with the results of the ECMWF reanalysis wave model (*left*) and the DWD forecast wave model (*right*). (Li et al., 2010)

ECMWF and the German Weather Service (DWD), both of which are based on the same basic physics.

The examples differ in two respects, however. First, as input first-guess spectra, the same predicted ECMWF spectra were used in both cases. Thus in the DWD case, the input data came from another model. Second, in the ECMWF prediction, in contrast with the DWD prediction, earlier SAR spectra had been

assimilated in initialising the wave spectrum for the subsequent wave model integration. Thus, it is not surprising that the deviations between the predicted and retrieved wave spectra are almost 50% smaller for the ECMWF model than for the DWD model. Attention must clearly be given to the relative weights assigned to the predicted first-guess spectrum and the SAR image spectrum both in the maximum likelihood retrieval algorithm and in the assimilation scheme when comparing predictions and observations. We return later to the important question of the advantages and disadvantages of combining prediction, retrieval and assimilation in a single operation, but first we present results in which no first-guess input wave spectra are used.

5. SAR Retrievals of Swell

In addition to the retrieval of the full wave spectrum, valuable information on the dynamics of ocean waves can be obtained from investigations of swell waves emanating from high-wind source regions. These are particularly suitable for global monitoring with SAR, as they propagate over large oceanic distances. Furthermore, if not too near the source of origin, they normally have sufficiently small steepness that the nonlinearities induced by velocity bunching can be neglected. Thus retrieval algorithms of type 1S or 2S can be used, independent of first-guess model predictions.

Following the early Seasat example of Lehner (1984; Fig. 2), Holt et al. (1998) reported similar results for ERS-1, in which swell waves emanating from an intense storm were tracked over a period of several days. Comparisons of SAR and buoy data indicated that SAR-derived peak wavelength and direction measurements could be used reliably to predict arrival times and propagation direction over large distances. A classic field experiment conducted by Snodgrass et al. (1966), who studied swell propagation along a great circle, and its attenuation during its crossing of the Pacific, was repeated by Heimbach & Hasselmann (2000). This time the authors used ERS-1 SAR retrievals over a 10-day period (Fig. 12, top right panel), together with spectra from ECMWF's WAM model collocated in time and space (top left panel) to assess the simulated swell properties. The retrieved and simulated spectra were traced back to their region of generation by a major storm off New Zealand (Fig. 12, bottom panels). A detailed comparison of the travel times of simulated and retrieved swells (in terms of their implied group velocities) revealed an underestimation of ECMWF's wind speed used to drive the wave model, a result that was confirmed independently by scatterometer data.

After 2002, the availability of operational complex SAR wave mode spectra from the Advanced SAR (ASAR) on Envisat stimulated the wider use of type 2S wave spectral retrieval algorithms, in which the directional ambiguity had been removed and the nonlinearities of velocity bunching (beyond the linear response approximation) were simply ignored. Since a first-guess wave spectrum, as in a type 2M algorithm, was now no longer needed to remove the directional ambiguity, but only to supply the information lost through the azimuthal cutoff by velocity bunching, the latter was simply ignored by restricting the application to spectra, such as swell, in which these effects were small.

Extensive comparisons of buoy data and the Envisat/ASAR wave mode Level 2 products (based on a mixed type 2S–2A retrieval algorithm; see Johnsen et al., 2006) were also carried out by Li & Holt (2009) using the UK operational wave model to interpolate between the locations and times of SAR and buoy measurements (Fig. 13). Figure 14 shows the comparison of model and Envisat/ASAR wave mode Level 2 products wave height at the Christmas Island (CI) buoy site in different spectral bins, i.e. wave periods. The agreement was satisfactory except for a median range of typical wind sea wave periods (10–16 s), in which the SAR retrieved wave height in this case was 25% higher than the buoy data.

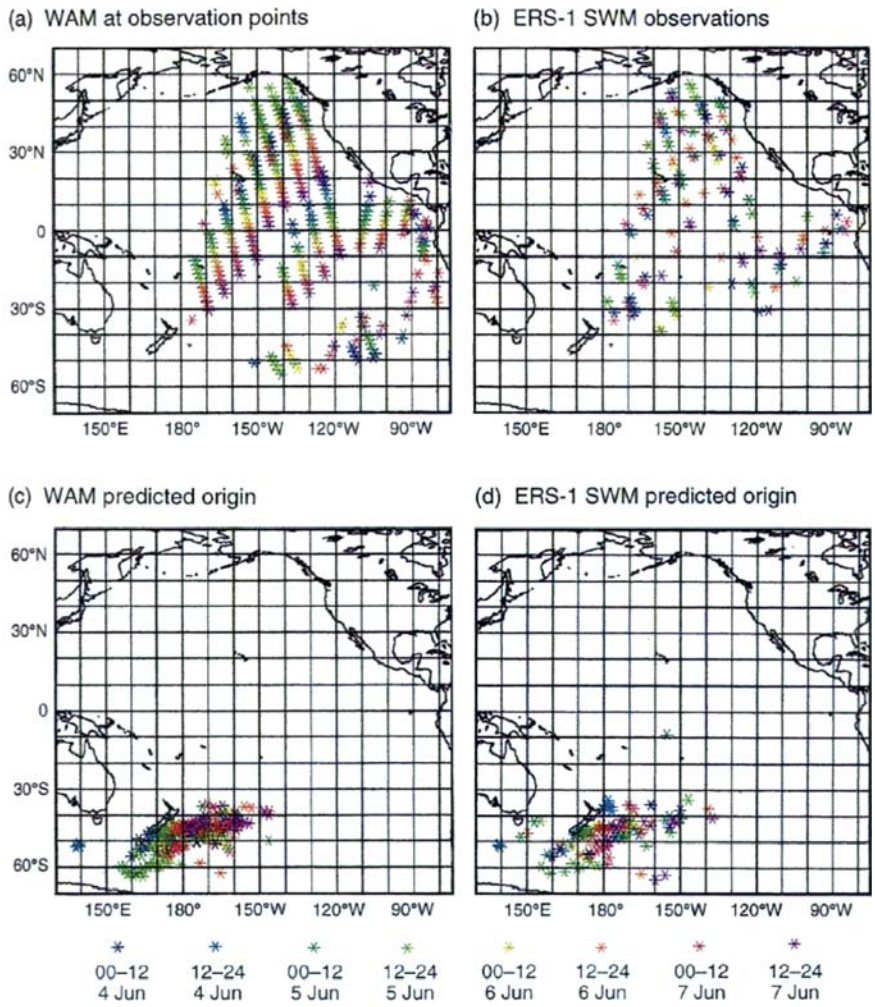

Figure 12. Simulated swell (*top left*) and SAR wave mode (SWM) retrieved swell (*top right*) propagating across the Pacific over a 10-day period. In the bottom panels, both simulated and observed swells are traced back to their regions of generation. (From Heimbach & Hasselmann, 2000)

Similar comparisons and cross-validations of the operational wave model against the ASAR wave mode Level 2 products have also been carried out by Météo-France. The Météo-France spectral retrieval is based on a partitioning and optimal interpolation algorithm applied to individual wave systems. The assimilation of one year (September 2005 to August 2006) of ASAR Level 2 wave products in the wave model WAM cycle 4 (Aouf et al., 2008) reduced significantly the rms error of the significant wave height. The impact of the assimilation is strongest in the tropics, where the sea is dominated by swell, and the weakest component of the wave model. Compared with the assimilation of Radar Altimeter wave heights, the impact of the assimilation of ASAR Level 2 wave spectra is most pronounced for longer-range forecasts from 12 to 60 h (Fig. 15).

Figure 16 shows a further example of the application of a type 2S retrieval algorithm, in this case to investigate the decay properties of long swells with periods of 13–18 s (Arduin et al., 2009). These wave components were and still are the largest source of error in global numerical wave models. The spectra from individual imagettes are sufficiently accurate to infer the dissipation rates of swell systems. Moreover, the large-scale consistency of the swell fields can be exploited to reach even more accurate estimates of characteristic wave parameters, by averaging wave properties in space and time. Ardhuin et al. (2009) found that the dissipation rates of swells were surprisingly nonlinear, with a stronger dissipation of steeper swells, and no clear dependence on the wave period or wind speeds (Fig. 16). This nonlinearity is consistent with the estimated strong dissipation rates for very steep swells derived by Högström et al. (2009).

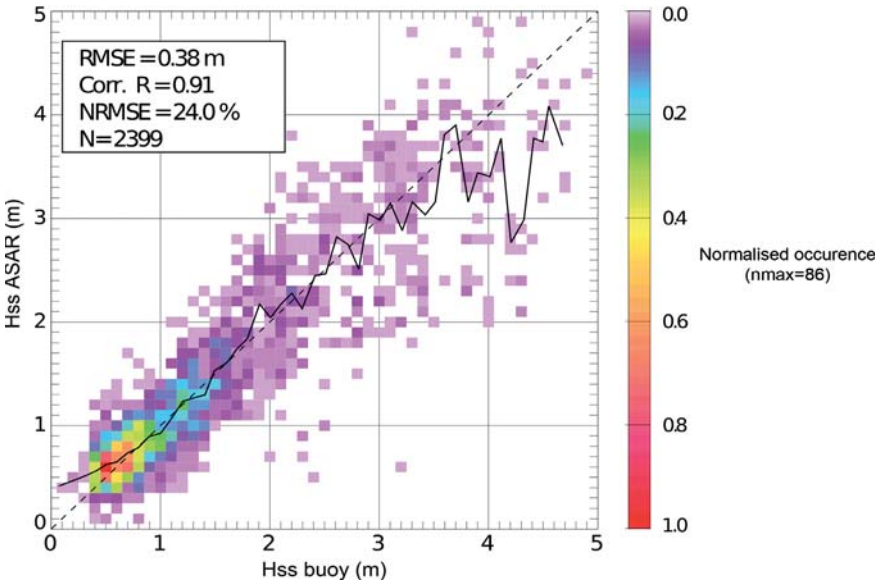

Figure 13. ASAR-derived versus buoy swell partition heights after bias correction, for the years 2004–8. The solid line joins the median values from SAR observations in each 0.1 m class of buoy-measured heights. (From Collard et al., 2009)

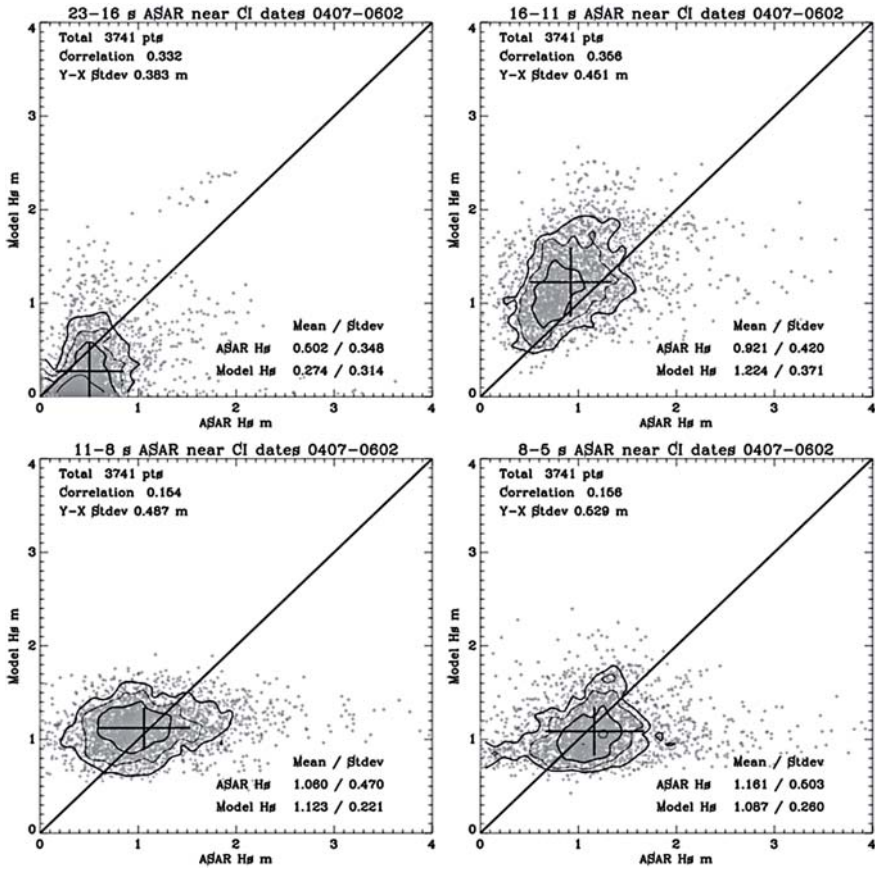

Figure 14. Comparison of model and Envisat ASAR wave heights at the CI buoy site in four spectral bins. (From Li & Holt, 2009)

Building on this observation, Ardhuin et al. (2010) used an analogy with the bottom boundary layer to parameterise nonlinear swell dissipation. The parameterisation is now used operationally by Météo-France and the Argentine Navy, and is being implemented by NOAA's National Weather Service and the National Centers for Environmental Prediction (NCEP) in the United States (Tolman et al., 2011).

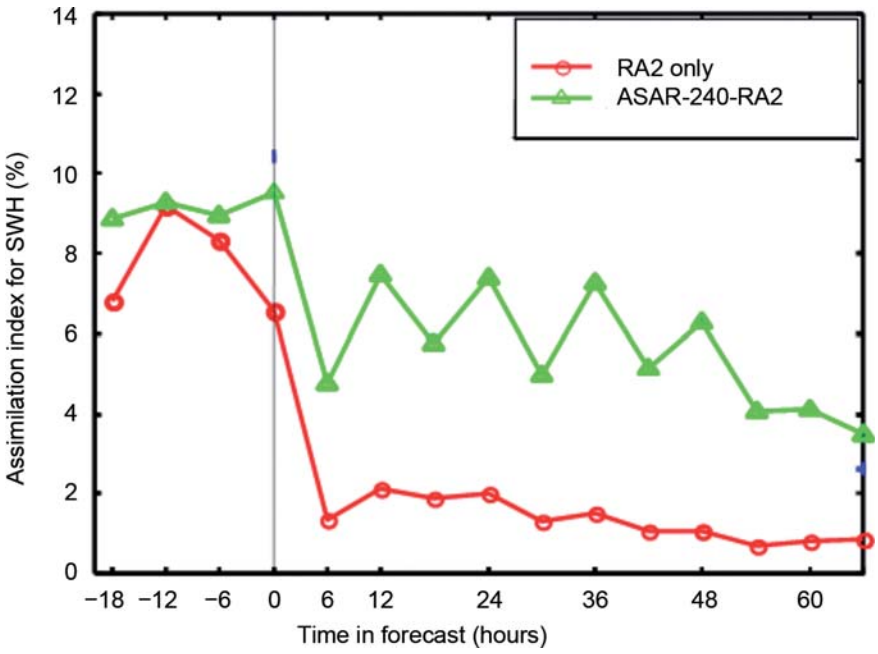

Figure 15. Variation in the assimilation index over the forecast period compared with Jason-1 wave heights. The red line indicates the assimilation of Radar Altimeter RA-2 wave heights only, while the green line refers to the assimilation of both RA-2 and ASAR Level 2 wave spectra. The assimilation index is the reduction of the rms error relative to the reference run without assimilation. (From Aouf et al., 2008)

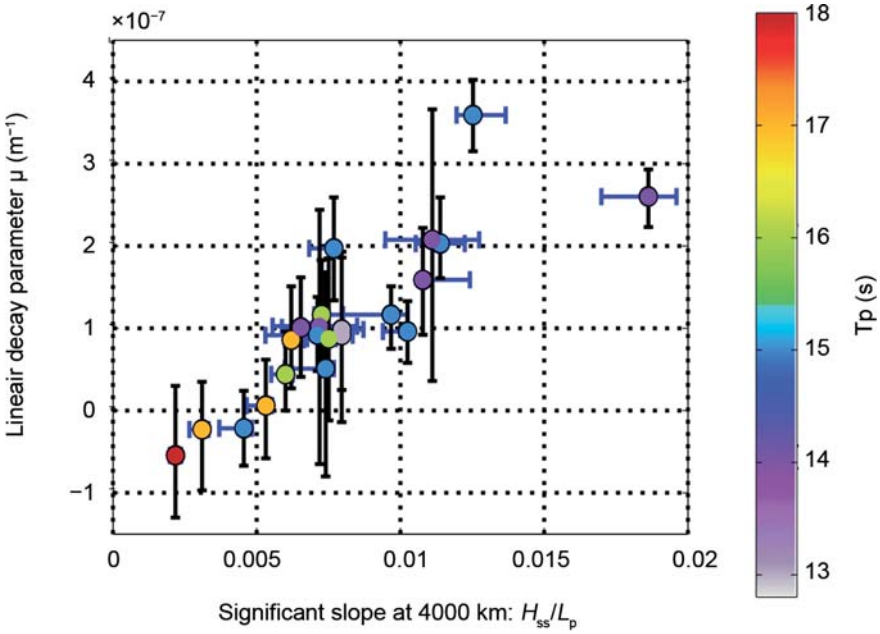

Figure 16. Swell dissipation for 22 swell events in the Pacific: estimated linear attenuation coefficient as a function of the swell significant slope (ratio of the swell significant wave height and peak wavelength, $s = 4\,H_s/L$), taken 4000 km from the storm centre, for a variety of peak swell periods (colours). (Ardhuin et al., 2009)

6. Globally Integrated versus Local Retrieval Algorithms

It is undisputed that second-generation retrievals, which use the complex information of the image cross-spectra to remove the directional propagation ambiguity, are inherently superior to first-generation retrievals using only SAR image variance spectra. However, this advantage is not pronounced in the combinations 1M and 2M, in which the first-guess input wave spectra from a state-of-the-art wave model can provide the necessary directional information (see, for example, Fig. 9, based on a type 1M retrieval algorithm).

The main advantage of second-generation retrievals comes to bear either in retrievals of type 2S, applied to swell-type spectra in which the azimuthal cutoff due to velocity bunching is insignificant (Figs 13–16), or in retrievals of type 1A and 2A, where the information lost through the azimuthal cutoff is

replaced by auxiliary data from sources other than a wave model. But even in retrievals of type 1S or 2S, the directional ambiguity is often not a serious problem, if the propagation directions (as in the examples presented above) can be clearly inferred from the overall geometry.

The main issue in the choice of retrieval algorithm therefore arises when the azimuthal cutoff becomes important, namely for steep, high-wind seas. The question is whether it is best in this case to use a first-guess wave spectrum provided by a state-of-the-art wave model (type 1M and 2M retrievals), or to try to substitute for the missing azimuthal cutoff information using other data (type 1A and 2A retrievals), such as from a radar altimeter, a scatterometer (although this instrument was no longer available on Envisat) or from wave buoys. The answer depends on whether the goal is to provide the best possible estimate of the wave spectrum, or to improve the wave model.

If the goal is to provide the best possible estimates of the wave spectrum for operational predictions or hindcasting studies, the answer is that one should clearly attempt to make optimal use of all available data in a global data assimilation scheme, including not only state-of-the-art wave models, but also state-of-the-art operational weather forecasting models, and all forms of observational data, including from satellites and conventional observing systems.

As an example, Figs 17 and 18 (Li et al., 2010) show the impact of assimilating first-guess model data on the prediction of a complex sea state in an intense storm region. It is clear that without a reasonably realistic first-guess input, it would have been impossible to derive the complex spectra shown on the right in Fig. 18 from the ESA WVW wave mode products shown in the middle column, which exhibit a pronounced azimuthal cutoff. But it is equally evident that the first guess for this complex storm system exhibits systematic errors that could not have been corrected without the information from the SAR. Thus a retrieval of the wave spectrum from the complex SAR image spectrum requires simultaneous information from both the SAR and the wave model.

On the other hand, if the goal is to test and improve the model, one should clearly strive to use independent data that have not been used in the model prediction. Unfortunately, this is feasible for SAR wave data only if one restricts the investigation, as in the examples of Figs 13 and 16 above, to type 1S and 2S retrievals, in which the nonlinear azimuthal cutoff region is excluded. In the case of strong wind sea spectra, as in the example just shown, the important spectral information lost beyond the azimuthal cutoff cannot be provided by model-independent, spectrally integrated observations. For this reason, most of the various proposed type 1A and 2A retrieval algorithms – e.g. Mastenbroek & de Valk (2000), CWAVE (Schulz-Stellenfleth et al., 2007), CWAVE_ENV (Li et al., 2011) – were not developed to test and improve state-of-the-art wave models, but rather simply to retrieve characteristic wave parameters.

Although these retrieval algorithms cannot therefore compete with type 1M and 2M state-of-the-art retrieval algorithms for detailed spectral wave measurements, or with type 1S and 2S algorithms for testing and improving state-of-the-art wave models, they nevertheless represent a valuable complement to these more sophisticated retrieval algorithms in providing generally accessible, simple tools for useful exploratory studies. As an example, Fig. 19 shows the validation of the operational wave model of the German Weather Service (DWD) against a combination of Envisat RA-2 data and ASAR-retrieved wave heights using the CWAVE_ENV algorithm.

In the long term, the SAR wave mode data could be seen as but one component of a highly complex satellite. The satellite, in turn, is only conceived as one component of an integrated Earth observation system, consisting of several satellites and an extensive ground-based conventional observing system. To make full use of this extensive global dataset, we need to develop sophisticated integrated models that also treat Earth as a complex coupled

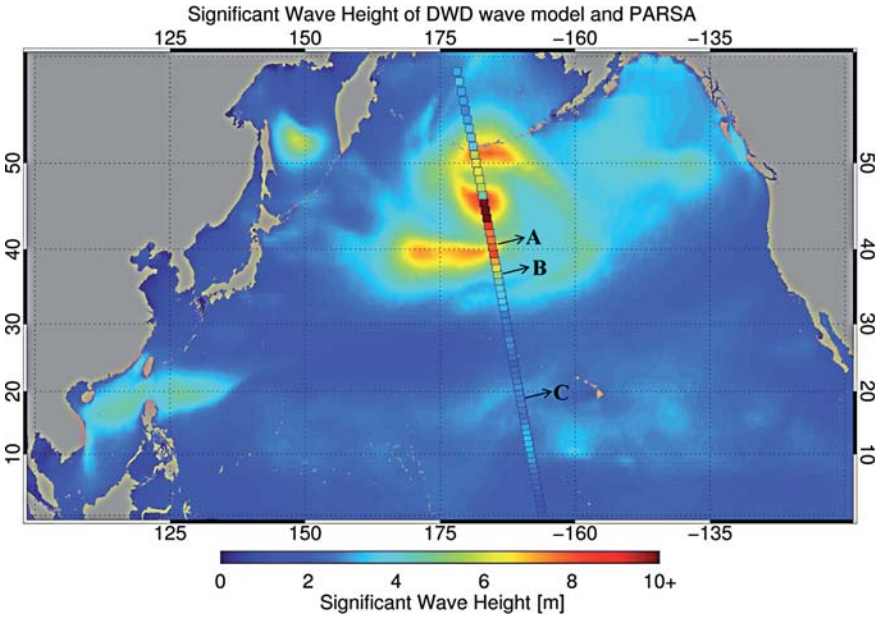

Figure 17. Locations of predicted and observed wave spectra at stations A, B and C within and south of an intense cyclone in the Pacific on 12 April 2009. (Li et al., 2010)

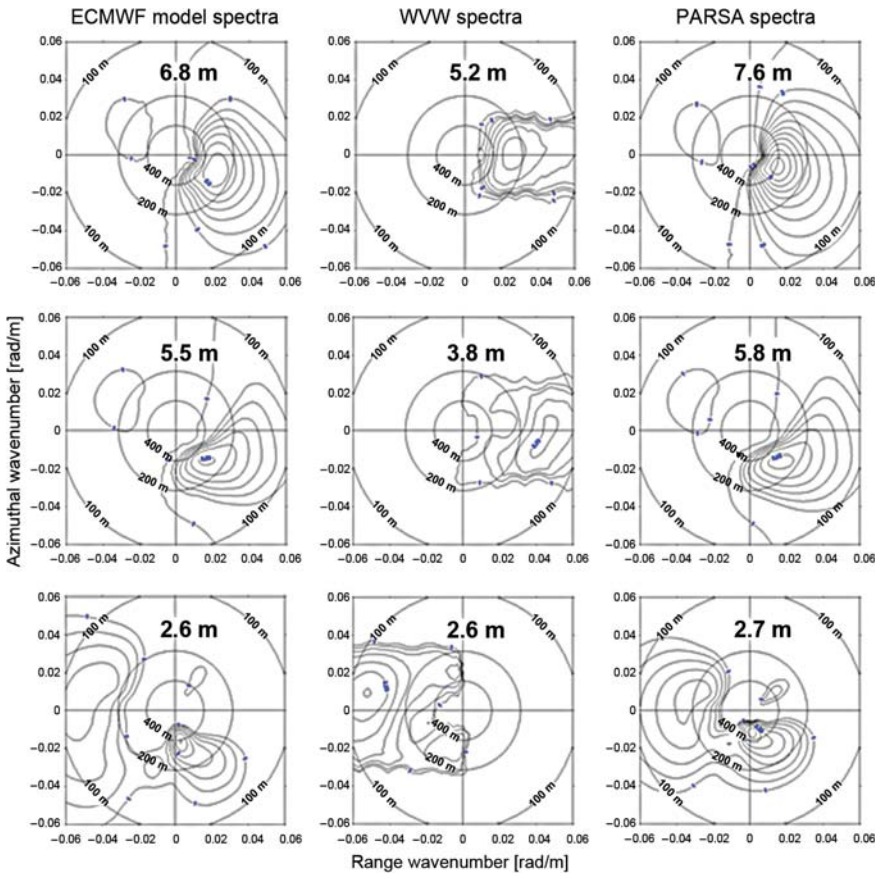

Figure 18. ECMWF predicted spectra (*left*), ESA SAR wave mode spectra (WVW) (*centre*) and PARSA retrieved spectra (*right*) for the three stations A (*top*), B (*middle*) and C (*bottom*) shown in Fig. 17. (Li et al., 2010)

system. In particular, the ocean wave field should be treated as an integrated component of the global weather system. The long-term goal should therefore be to assimilate the SAR wave data together with all other relevant sources of data (radar altimeter wave heights and winds, standard meteorological data, ocean buoy data, etc.) within a state-of-the-art integrated global atmospheric and ocean wave forecasting system. Within this general framework, a future ERS–Envisat–Sentinel integrated assimilation system should be extended to include also ocean currents (see section 8).

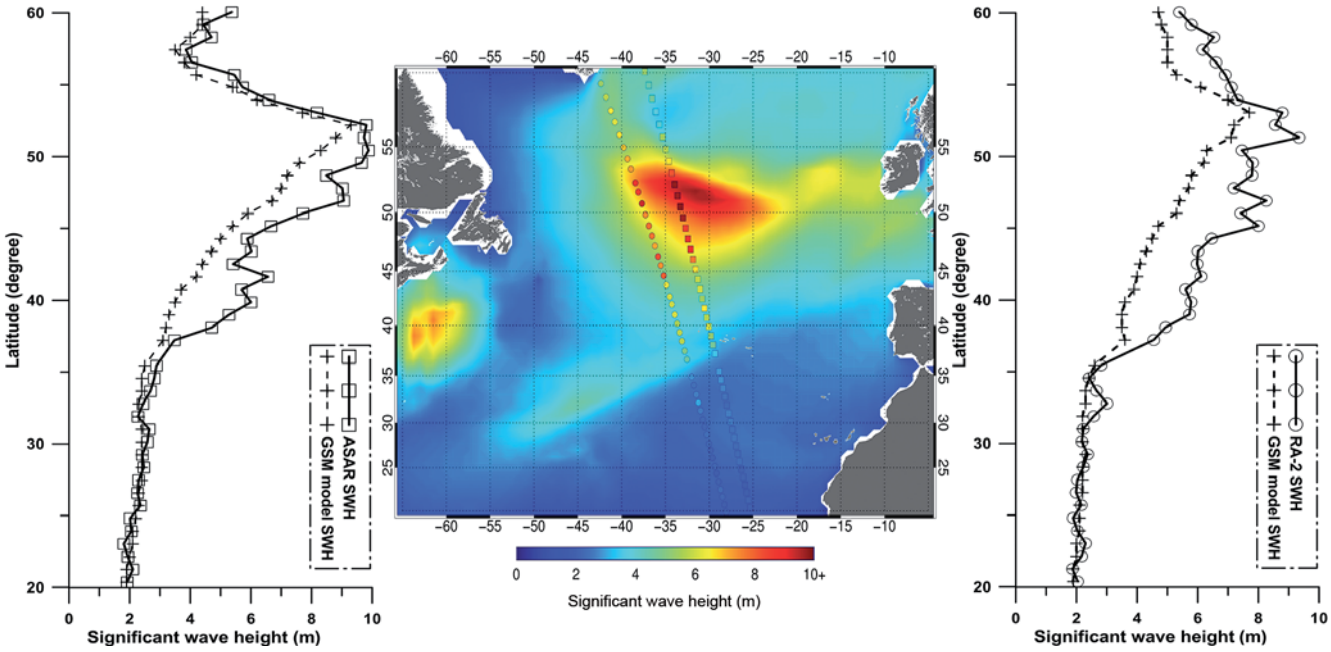

Figure 19. Validation of the DWD forecast wave model using simultaneous wave measurements of the Envisat/ASAR and RA-2. *Centre:* The forecast wave field at 0:00 UTC on 20 January 2007 (background) and significant wave heights (SWH) retrieved from the ASAR wave mode data using the CWAVE_ENV algorithm (right track), and the collocated RA-2 SWH data (left track), both acquired between 23:39 and 23:51 UTC on 19 January 2007. The right and left panels show the model predicted SWH compared with the ASAR and RA-2 retrievals, respectively. (Courtesy of X.-M. Li)

In summary, the 20 years of SAR wave mode data provided by ERS-1 (1991–2000), ERS-2 (1995–2011) and Envisat (2002–2012) have had a major impact on ocean wave research and operational numerical wave prediction. The satellites produced invaluable data on the two-dimensional ocean wave spectrum that no other instrument was able to provide at a comparable level of spectral resolution and global, continuous coverage. The dataset has been indispensable for improving and validating the global wave model WAM (WAMDI, 1988), which is now applied in over 200 research and operational forecasting centres worldwide, as well as for improving similar wave prediction models operated by the French, UK and US weather services. Implemented together with the radar altimeter wave heights in the data assimilation mode, the wave mode SAR data have significantly improved, and can be expected to further improve, the quality of wave prediction.

7. Ongoing and Future Research

Apart from their invaluable contribution to the determination of global ocean wave spectra, SAR wave mode data also have other applications that are the subject of current and planned future research. These include investigations of extreme sea states in intense storms, studies of individual exceptional wave states, such as freak (monster) waves, and the extension of numerical wave models in the general context of Earth system modelling, including the improved representation of wave–current interactions, air–sea fluxes, and second-order spectral quantities related to infra-gravity and microseism generation.

7.1 Extreme Sea States

Both tropical cyclones, which are associated with the most intense winds and air–sea fluxes, and extratropical cyclones, which produce most of the highest sea states, are difficult to observe directly due to sampling and signal saturation issues. Yet, these storms define the design criteria for most ocean engineered structures and coastal defences. Satellites provide a unique opportunity for overcoming these sampling problems. For instance, the largest significant wave height recorded by a satellite altimeter reached 20.1 m when storm Quirin crossed the North Atlantic in February 2011. A joint analysis of the remotely sensed winds and waves, including Envisat/ASAR data, confirmed the existence of very long waves, with peak periods reaching 25 s, supported by *in situ* buoy measurements and the analysis of seismic noise at land-based stations (Hanafin et al., 2012).

To understand the dynamics of such extreme wave systems, it is important to observe both the conditions within the high-wind region itself and the long swell components emanating from the storm, which allow conclusions to be drawn on the processes within the storm itself (see examples presented in Figs 14–16). Data for both regimes can be provided by the global SAR wave mode observations. A careful combination with seismic noise data should yield further insights into the evolution and statistics of these extreme events (Grevemeyer, 2000; Aster et al., 2008; Ebeling & Stein 2011).

The evolution of the wave spectrum within an intense storm region is governed by four processes: wave propagation, the energy transfer due to resonant nonlinear wave–wave interactions, wind generation and dissipation by white capping and turbulence (Komen et al., 1996; Janssen, 2008). Of these, the first two are completely understood theoretically from first principles and are free from empirical constants, while the last two are represented in wave models by empirical expressions tuned against extensive observed wave growth data. The most important process for the structure of the wave spectrum is the nonlinear energy transfer, which redistributes the energy within the spectrum through resonant interactions between wave quadruplets and is responsible for the formation of a sharp spectral peak that gradually shifts to lower frequencies (longer wavelengths) in a growing wind sea.

Unfortunately, although the nonlinear energy transfer is well understood theoretically, and has been computed numerically in a number of case studies, the exact transfer expression is represented by a three-dimensional integral that is impossible to compute exactly for each frequency, direction and spacetime point of a numerical wave model. Most models therefore use a strongly simplified expression, the Discrete Interaction Approximation (DIA) based on a single dominant wave quadruplet (Hasselmann et al., 1985) that reproduces the principle properties of a growing wind sea in a uniform wind field, but is known to exhibit serious deficiencies under more complex wind conditions. With the advances in computing power since the DIA was first introduced, a number of improved versions of DIA including more basic interaction quadruplets have now been proposed (e.g. van Vledder, 2001; Tolman, 2004, 2009, 2011; Ueno & Kohno, 2004; Tamura et al., 2008, 2010). The data derivable from the ESA SAR wave mode using type 2M retrieval algorithms provide excellent new opportunities for testing the impact of these suggested improvements, in combination with the assumed wind input dissipation source functions, under realistic extreme wind conditions (as illustrated by the example in Figs 17 and 18).

Nonlinear interactions, wind action and dissipation processes can still be important a few storm diameters outside an active generating area. They lead to a redistribution of the wave energy leaving the storm (Snodgrass et al., 1966), which can then be detected in the swell propagating away from the storm over very large distances. The swell systems can be readily observed with the SAR using simpler type 2S retrieval algorithms. Apart from avoiding

the complexities of 2M retrievals associated with the admixture of predicted and observed data, these measurements have the advantage that the swell systems can be tracked over much larger areas of the ocean. As well as reconstructing the location and time of the storm, the measurements can then provide valuable indirect information on the processes active within and in the vicinity of the storm area. Preliminary investigations (Delpey et al., 2010) have found, for example, that swell can be detected with the SAR wave mode propagating away from the storm in directions perpendicular to the principal swell propagation direction. It is not yet clear whether this is controlled by the variability of the wind fields in a storm, by the variable directional spectral shapes in the storm, or by directional spreading through nonlinear wave–wave interactions. A combination of storm-related swell data using type 2S SAR retrievals and type 2M retrievals for the storm area itself could yield important new insights into the nature of extreme sea states in severe storms.

7.2 Freak Waves

The occurrence of extreme individual waves, called freak or monster waves, has become a major concern because of the rapid increase in global trade and the concurrent growth in global shipping using ever larger container vessels. It has been estimated that in recent years an average of about one super-container ship carrying many thousands of containers has been lost per month. Although the cause of the loss is often unknown, it is suspected that in many cases it was due to an unexpected encounter with an individual monster wave (Fig. 20).

Although long attributed to the narrative lore of seamen, the reality of monster waves has now been clearly established through many well documented reports. While they are obviously difficult to interpret directly due to the intrinsic nonlinear imaging property of the SAR instrument, unusual wave formations have also been identified in SAR wave mode images, opening up the possibility of obtaining information on the probability of the occurrence of freak waves using the global observing capability of the SAR wave mode.

However, to relate SAR data to freak waves, three major problems must first be resolved: What is the physical structure of a freak wave? Given the physical structure of a freak wave, how is this very nonlinear, rapidly moving individual surface feature mapped into a SAR image? How can one invert the mapping to recover the original freak wave from the SAR image?

Regarding the first question, the simplest hypothesis is that a freak wave can be described to first order as the straightforward linear superposition of

Figure 20. Monster wave encountered by the NOAA ship *Discoverer* in the Bering Sea, 1979. (Commander Richard Behn, NOAA Corps)

the individual wave components of a random sea state. Freak waves would then obey Gaussian statistics. However, the available evidence suggests that observed monster waves can be considerably higher than can be reasonably expected from Gaussian statistics, and must thus therefore represent a basically nonlinear phenomenon. Various nonlinear models based on the Benjamin–Feir wave–wave interaction instability mechanism (Janssen, 2003) or on wave–current interactions have been proposed, but it is likely that a number of different nonlinear interaction configurations can produce freak waves (Dysthe et al., 2008).

Given the structure of a freak wave, including the orbital velocity field and its interaction with the short backscattering Bragg waves superimposed on the large-scale orbital velocity field, the mapping into a SAR image is in principle well defined (although for ERS SAR wave mode incident angles of only 23°, the standard Bragg backscattering theory must presumably be augmented for steep range-travelling waves by a specular reflection model). However, the computation of the resultant image is computationally demanding. Unfortunately, the statistical closure methods applied in the fully nonlinear forward-mapping algorithm of Hasselmann & Hasselmann (1991) and Krogstad (1992) for wave spectra cannot be simply carried over to the case of individual wave representations.

However, an approximation using a linearised Fourier transform relation for individual images, in which a filter is applied to the azimuthal cutoff region (corresponding to a type 2S algorithm, but applied now to the image itself, not to the image spectrum), has been proposed by Schulz-Stellenfleth & Lehner (2004). Figure 21 shows an example of the sea surface elevation field (B) derived from the calibrated ERS-2 wave mode data (A) using this algorithm. The algorithm has been applied to two years (September 1998 to November 2000) of reprocessed ERS-2 SAR wave mode data to derive a global map of maximum (SAR estimated) single wave heights (Fig. 22). Although not applicable for quantitative assessments of individual wave heights, due to the neglect of the nonlinear distortions induced by the SAR imaging system, this provides nevertheless a useful tool for arriving at first estimates of the statistics of exceptional individual wave occurrences as seen by the SAR.

Another application of SAR-derived wave images is the investigation of wave groupiness (Borge et al., 2004; Niedermeier et al., 2005). Figure 23 shows an example of pronounced wave groupiness occurring in the vicinity of the Ekofisk oil platform in the North Sea.

The third and final challenge is to invert the freak wave → SAR image mapping relation in order to recover the properties of the original monster wave from the SAR freak wave image. This will depend, of course, on the freak wave model and will presumably involve some form of parametric inversion method. Without progress in addressing the first two problems, however, predictions on advances on this question must remain speculative.

Even after a complete three-stage freak wave model → SAR freak wave image → SAR image inversion scheme has been developed, one then faces the further difficulty that the probability of simultaneously observing a freak wave both in reality and in a SAR wave image in order to validate the model is for all practical purposes negligible. However, there is an interesting exception: the monster waves that occur at a few locations famous for their exceptional surfing conditions (Fig. 24). These huge surf waves are produced by refraction at subsurface reefs and are generated under well defined, reproducible and measurable wave conditions. Although representing a special type of monster wave, they may provide an ideal dataset for testing theories of the mapping of monster waves into SAR images, as well as for developing the associated inversion algorithms. Under less extreme conditions, coastal wave transformation due to complex bathymetry changes can also be used to interpret and better understand SAR observations involving wave focusing and refraction effects (e.g. Collard et al., 2005).

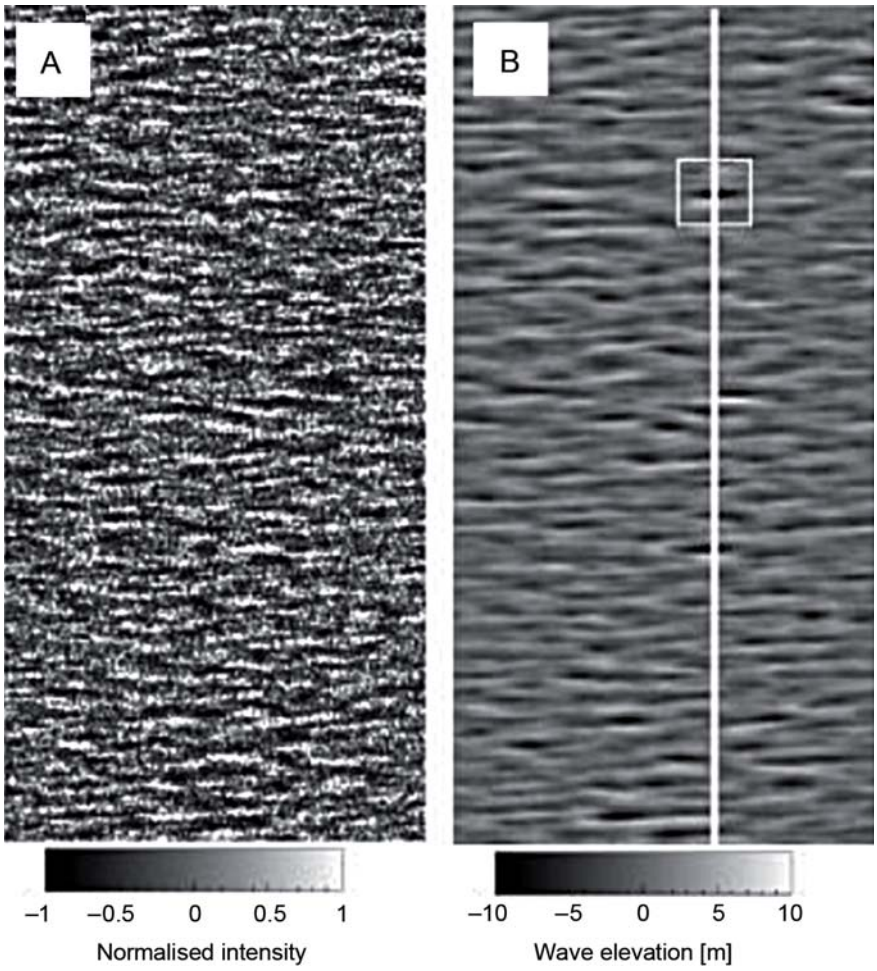

Figure 21. SAR ocean wave retrieval in the spatial domain. A: A 5 × 10 km normalised ERS-2 SAR wave mode imagette acquired at 48.45°S, 10.33°E on 27 August 1996. B: The retrieved sea surface elevation field. (From Schulz-Stellenfleth & Lehner, 2004)

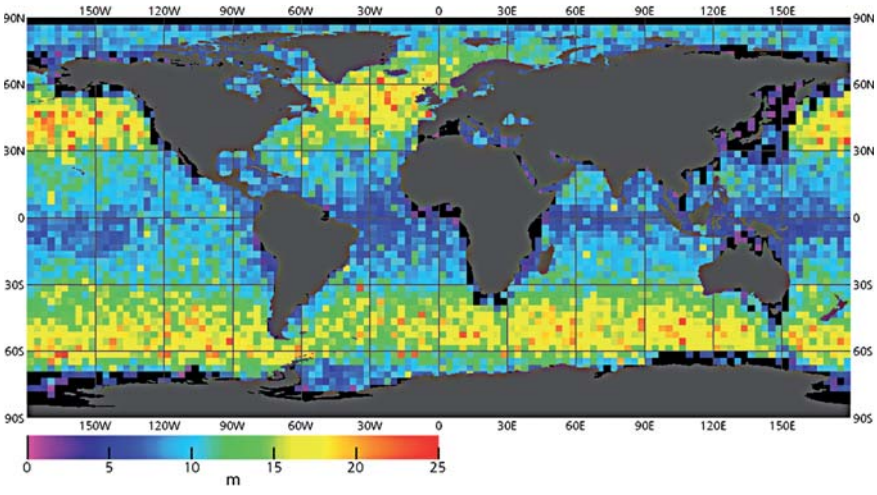

Figure 22. Estimated maximum individual wave heights inferred from ERS-2 SAR wave mode data acquired between September 1998 and November 2000. (Koenig et al., 2007; DLR)

In summary, most SAR wave observations have been motivated by the desire to improve our understanding and prediction of wave spectra, with less attention paid to the imaging of the individual wave fields themselves. However, the representation of individual waves can yield important information not only on freak waves, but also on other phenomena, such as wave grouping, the transformation of waves in the surf zone, and non-Bragg microwave returns from fast scatterers or reflectors, for example, from white caps or steep waves.

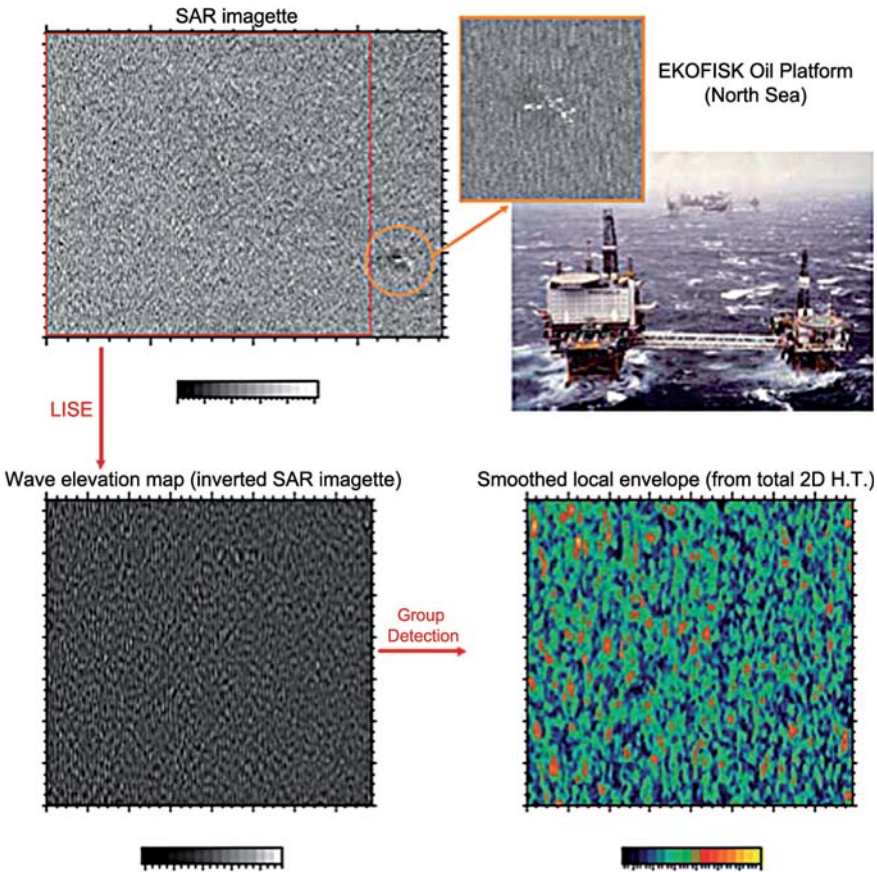

Figure 23. Analysis of wave groupiness in the area of the Ekofisk oil platform in the North Sea. (From Borge et al. 2004)

Figure 24. A monster wave off Hawaii. Such surf waves pose no immediate danger to shipping, but are ideal for testing theories of the mapping of monster waves into SAR wave images, together with their associated inversion algorithms. (EPA)

7.3 Wave–Current Interactions

Ocean waves propagating through strong, variable currents can undergo dramatic changes in wave height and steepness. In a steady shear current, wave rays are bent, the bending being proportional, in the approximation of geometric optics, to the ratio of the vertical component of the current vorticity to the wave group velocity. Thus refraction effects become important whenever surface gravity waves propagate through major ocean currents exhibiting high gradients. Particularly critical are frontal zones, which can lead to wave

reflections, trapping and waveguide propagation of the trapped wave within the current. The resulting wave field can become very complex, with wave systems following different paths, producing crossing seas and caustics. The resultant strong spatial variations in wave energy can seriously endanger navigation. The effects have been observed in numerous SAR images; Liu et al. (1994), for example, carried out an empirical analysis of wave ray refraction patterns inferred from an ERS-1 SAR image over an ocean eddy.

Most of these data have not been supported by synchronous measurements of surface currents.

Today, however, routine ocean circulation models are available that assimilate multi-satellite altimeter sea surface height data, thereby better characterising the mesoscale upper-ocean dynamics and enabling the incorporation of wave refraction effects in wave models. Wave–current investigations using SAR observations can furthermore be enriched through an emerging analysis capability to infer ocean surface velocities directly from the Doppler information of the SAR data themselves (Chapron et al., 2005; Johannessen et al., 2008).

As an example, Figs 25 and 26 illustrate the deflection of waves by large surface current gradients in the Agulhas current off the coast of South Africa, detected using the Envisat wide-swath SAR data. The currents (Fig. 25) were determined using the SAR Doppler information, while the wave spectra (Fig. 26) were obtained using a 1S retrieval algorithm (2S retrieval algorithms free from directional ambiguities were not directly available for the full-swath SAR data, as ESA provides the required complex image spectra only for the SAR wave mode imagette data). The incoming swell propagation rays are seen to be strongly deflected by the large current gradients, producing crossing-swell systems from an initially uniform incoming swell system within only 200 km.

The problem of wave–current interactions is closely related to that of wave–wave interactions, and both can be invoked to explain the generation of spacetime caustics and anomalous wave systems, including freak waves as an extreme case. In general, waves are scattered and amplified when propagating in an inhomogeneous random medium, which can represent a nonuniform, slowly varying current, as in the above example, or the low-frequency, low-wavenumber random currents that are continuously generated in a random sea state by quadratic difference interactions between different wave components. From this perspective, the Benjamin–Feir instability invoked to explain the generation of extreme waves (Janssen, 2003) can be placed within the general theory of unstable wave–wave interactions (Hasselmann, 1967) in a form analogous to the wave–current interaction mechanism considered above.

Finally, quadratic wave–wave interactions between wave components of nearly the same frequency propagating in opposite directions generate microseisms (Longuet-Higgins, 1950; Hasselmann, 1963). Precisely measured microseismic records can be used to determine the arrival times of different swell components. Using geometric optics, the source can be determined with high accuracy by triangulation from several seismic stations (Fig. 27; Husson et al., 2012).

Waves propagating in opposite directions with the same frequency occur only infrequently in the open ocean and are usually an indication of an unusual storm event, such as an intense tropical or mid-latitude cyclone, or possibly effects of multiple wave–current refractions. As recently demonstrated (Ardhuin et al., 2010), numerical model of microseism generation by random ocean waves, including ocean wave reflections, are becoming increasingly realistic. Yet, the development of microseism observations into a reliable early warning system and/or the full exploitation of available 50 years of seismic data archives still require more detailed knowledge of the directional properties of ocean wave spectra than is presently achievable using the energy transfer parameterisations (as discussed above) applied in current state-of-the-art wave prediction models. The extensive global directional wave information made available by the two-dimensional ERS–Envisat wave mode data should again prove invaluable in investigating this attractive option.

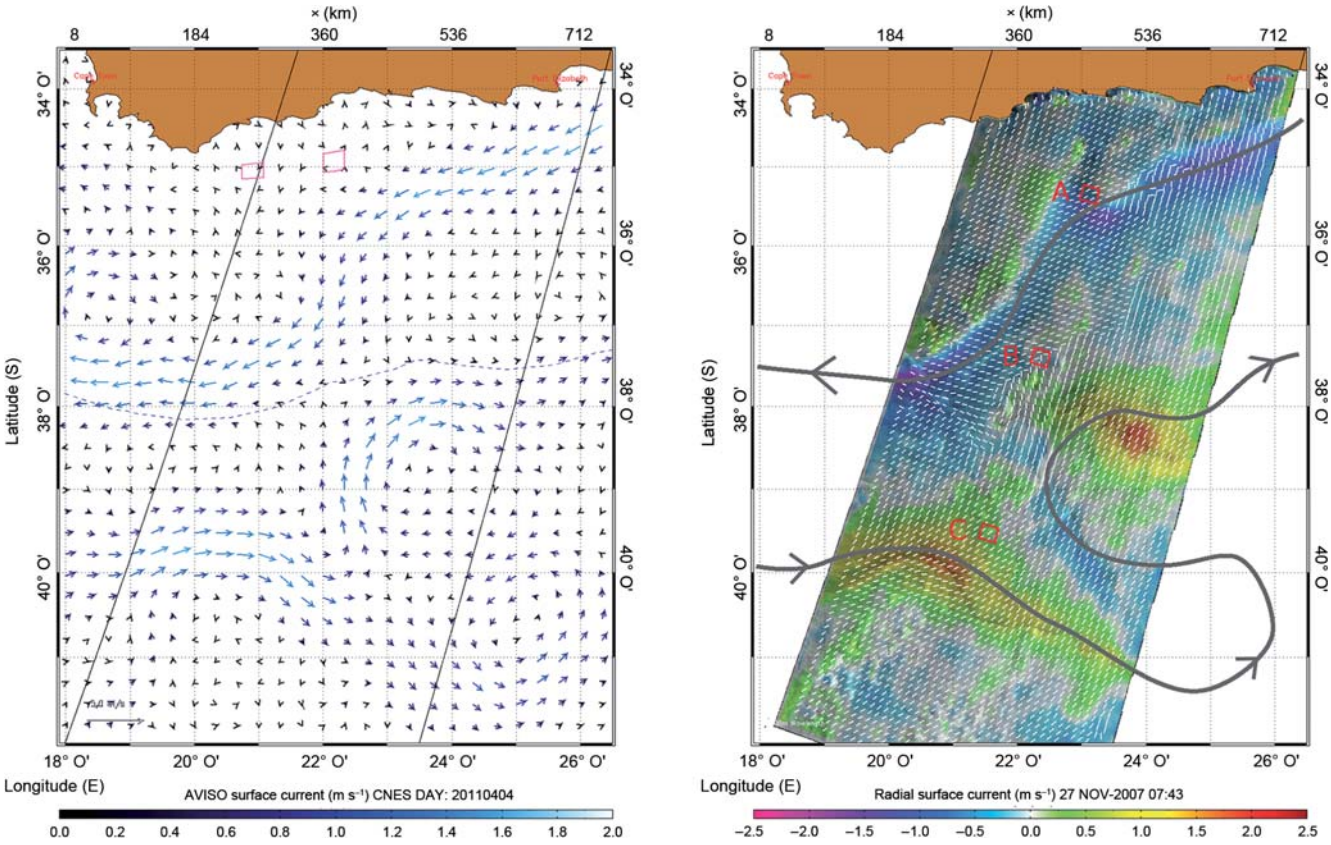

Figure 25. Envisat/ASAR-derived currents and wave observations in the Agulhas current (*left*), confirmed by the altimetry-derived surface flow field (*right*). A southwesterly swell system interacts first with the Agulhas current, flowing toward the west, and subsequently with the Agulhas return current, flowing and meandering towards the east. The principal swell propagation directions (*left*) are displayed as background below the sketched ASAR Doppler-derived current pattern (full curves). (CLS)

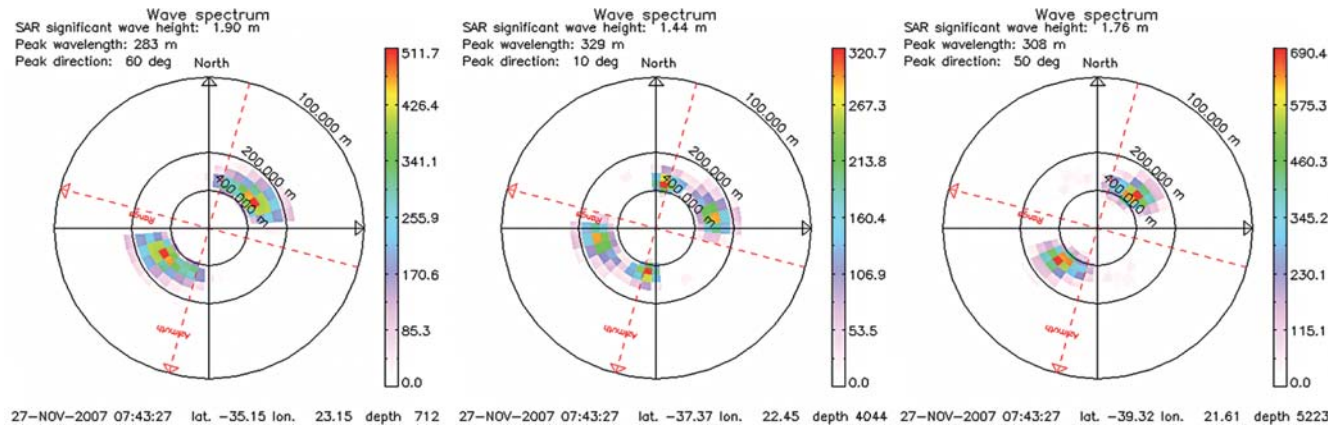

Figure 26. Wave spectra for three imagettes corresponding to the three locations shown in Fig. 25: A (*left*), B (*middle*) and C (*right*). The 300 m swell system is strongly influenced by the large surface current gradients, and the two swell patterns of comparable energy eventually cross. (CLS)

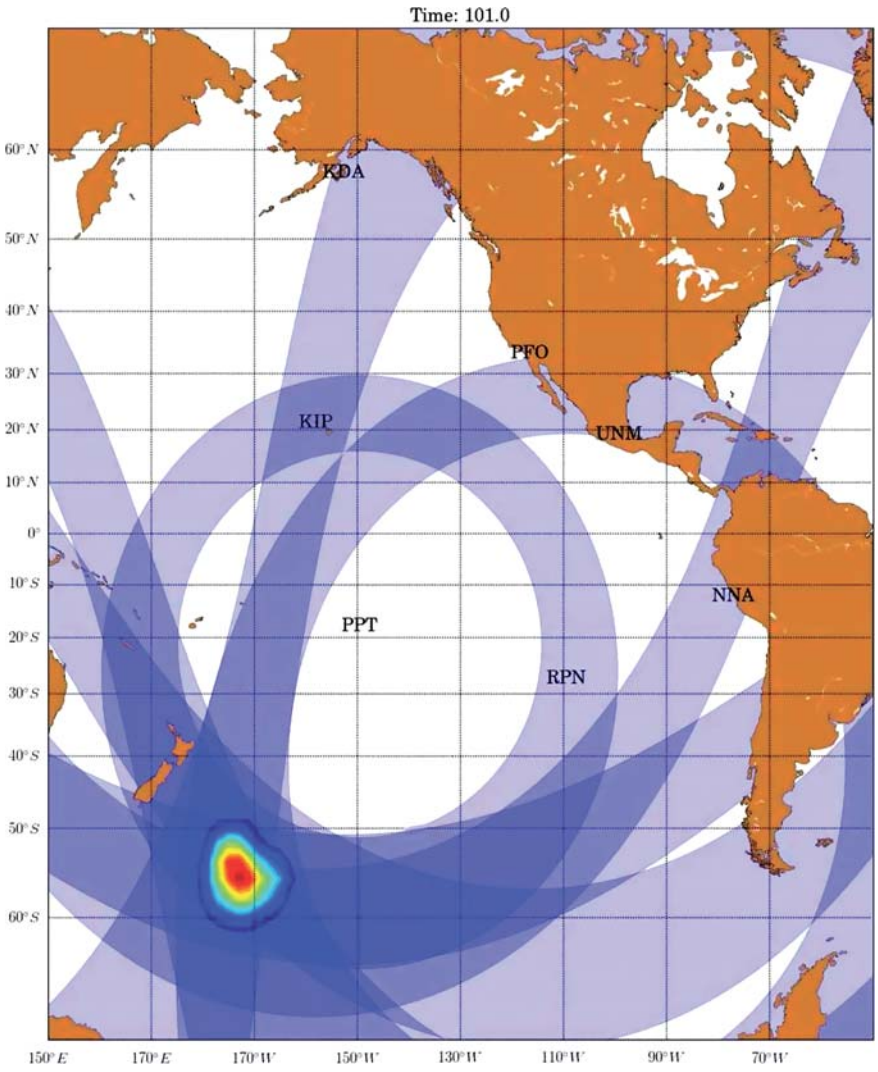

Figure 27. Location of an expected storm source from independent SAR wave mode products and seismic noise measurements. For each seismic station, a 1000-km wide blue disc has been plotted with a radius equal to the distance to the storm source, as estimated from the differential arrival time of the swell at the seismic station. The different discs intersect southwest of New Zealand, in agreement with the storm location given by the SAR (the red dot is the location at which backward-propagated SAR measurements converge). (From Husson et al., 2012)

8. Conclusions and Outlook

The sequence of ESA satellites ERS-1, ERS-2 and Envisat deployed over the last 20 years has had an immeasurable impact on oceanography, meteorology and climate research. We have focused in this chapter on the dynamics and prediction of ocean waves, in particular on the information provided by the ERS SAR wave mode component of the Active Microwave Instrument (AMI). However, since ocean waves are generated by the wind, interact with ocean currents, generate microseisms, affect coastal and offshore structures, and influence shipping and navigation, an improved understanding and prediction of ocean waves is important for many other aspects of the Earth system. Thus, the ERS SAR wave mode, designed to provide global measurements of the two-dimensional ocean wave spectrum, must be seen as an integral component of a global Earth observation scheme, consisting not only of the full complement of ERS instruments, but also of many other satellites providing data on ocean currents, surface winds and other oceanic and atmospheric variables, including also the extensive system of conventional *in situ* measurements.

The impressive series of publications based on the ERS SAR wave mode instrument (of which only a selected subset has been cited here) illustrates the complexity of the problems that need to be addressed in order to exploit the full potential of the instrument. The ERS satellite was conceived in the late 1970s, when the oceanic community had just developed realistic numerical models of the two-dimensional ocean wave spectrum for operational global

wave prediction and eagerly welcomed the opportunity to feed these models with appropriate wave spectral data from a globally observing satellite. However, although Seasat had already demonstrated that a SAR could image ocean waves, it soon became apparent that the imaging process was highly complex. For a quantitative interpretation of the ERS SAR wave images, detailed models of the electromagnetic return from a random, moving surface, including, in particular, the interactions between short backscattering Bragg waves in the decimetre range and the imaged long waves in the 100–1000 m range were needed. These were soon developed. Methods were then needed to invert the mapping relation, and retrieve the two-dimensional wave spectra from the satellite image spectra. This task was also achieved. However, because the general forward-mapping relation was nonlinear, the inverse mapping relation involved the unavoidable loss of some information: wavenumbers beyond an azimuthal high wavenumber cutoff could not be resolved. Thus, for a satisfactory general retrieval algorithm, the missing spectral information needed to be supplied from another source. In practice, the only available source was a two-dimensional spectral wave model, as all conventional measurement systems (other than wave buoys at a few isolated locations) are unable to resolve the specific spectral bands of interest. Thus retrieval algorithms in the general nonlinear case necessarily require an input first-guess wave spectrum from a wave model.

This results, however, in an unavoidable intertwining of three separate aspects of the ERS SAR wave mode data: the retrieval of ocean wave spectra from the SAR data, the prediction of ocean wave spectra, and the assimilation of observational data in wave prediction models. The last two aspects imply that the application of the SAR wave mode data becomes coupled also to the problem of weather prediction, involving in addition the measurement and assimilation of atmospheric data. The separability of the three problems is feasible only for swell systems, outside an active wave generation region, in which the nonlinearities of the SAR imaging mechanism become negligible.

The application of SAR wave mode data in this intertwined mode, together with improvements in weather prediction and associated atmospheric data assimilation methods, has led to the continuous improvement of global wave prediction models to a level at which, for most state-of-the-art wave models today, no systematic deviations between observed and modelled wave spectra, beyond the expected variability of observations, is found in the overall statistics of the comparisons of model predictions and SAR observations.

However, significant deviations can still be found in individual cases, such as in intense cyclonic storms. Apart from the difficulties of an accurate prediction of wind fields in such extreme situations, it is well known from theoretical studies that the numerical approximations of the important source function describing the nonlinear energy transfer exhibit serious shortcomings in most wave models in complex wind seas. The SAR wave mode data provide an excellent opportunity for revisiting this problem and significantly improving wave models in these important cases.

A related problem in which the application of SAR wave mode data could lead to significant progress is in the occurrence of individual extreme wave formations known as freak or monster waves. Although monster waves occur infrequently, they represent a serious danger for the rapidly expanding global shipping industry, causing significant losses or damage to container ships and supercarrier vessels. Global SAR wave mode observations of individual extreme waves could provide a valuable statistical database for determining the frequency and conditions of occurrence of these poorly understood wave formations. However, further work is needed on the nonlinear SAR imaging of individual waves before a quantitative determination of the statistics of real freak waves rather than freak SAR wave images can be provided.

Another process that leads to the formation of extreme wave conditions is the interaction between waves and currents, an important problem that is also

ripe for a more detailed exploration using SAR wave mode (and in this case also full-swath SAR data). Strong current gradients can result in a focusing of waves, producing abnormal wave conditions. Previously regarded as largely unpredictable, the simultaneous measurements of both wave spectra and currents using SAR wave imaging, the SAR Doppler for current measurements, and currents computed from radar altimeter sea level measurements, now enable predictions of the anomalous wave spectra produced by wave–current interactions.

Finally, interesting data on the location of unusual systems of ocean waves travelling in opposite directions can be derived from triangulations of microseism measurements at different stations. Microseisms of twice the wave frequency are generated by quadratic interactions between ocean waves travelling in opposite directions in the open ocean, caused by moving cyclonic storm systems, or in the vicinity of coasts through wave reflections at steep shorelines. Important indirect information on processes within a storm can also be derived from observations of swell propagating away from a distant storm.

These and other examples presented in this chapter demonstrate that despite the considerable advances in our understanding and prediction of ocean waves achieved through the ERS SAR wave mode data, many interesting problems that could be successfully addressed using this instrument still await a solution.

It is therefore very encouraging that there are plans to continue the ERS-1/ERS-2–Envisat satellite system with the launch in 2013 of Sentinel-1, the first in a series of next-generation satellites, as an important component of the Global Monitoring for Environment and Security (GMES) system. Sentinel-1 will again carry a SAR wave mode instrument with enhanced capabilities (20 × 20 km imagettes every 100 km). The continuation of this satellite series is important not only for the upgrading of the present ocean observing system and the resolution of the open problems mentioned, but also for the creation of a long-term time series in support of climate change monitoring.

References

Abdalla, S., Bidlot, J. & Janssen, P. (2004). Assimilation of ERS and ENVISAT wave data at ECMWF, *Proc. 2004 Envisat & ERS Symposium*, Salzburg, Austria. ESA SP-572, European Space Agency, Noordwijk, the Netherlands.

Abdalla, S., Janssen, P. & Bidlot, J.-R. (2010). Envisat ASAR wave mode spectra global validation and assimilation. *Proc. SeaSAR 2010*, Frascati, Italy. ESA SP-679, European Space Agency, Noordwijk, the Netherlands.

Alpers, W.R. & Rufenach, C.L. (1979). The effect of orbital motions on synthetic aperture radar imagery of ocean waves. *IEEE Trans. Antennas Propagat.* **27**, 685–690.

Aouf, L., Lefevre, J.-M., Chapron, B. & Hauser, D. (2010). Some recent improvements of the assimilation of upgraded ASAR L2 wave spectra. *Proc. SeaSAR 2010*, Frascati, Italy. ESA SP-679, European Space Agency, Noordwijk, the Netherlands.

Ardhuin, F., Chapron, B. and Collard, F. (2009). Observation of swell dissipation across oceans. *Geophys. Res. Lett.* **36**(L06607), 10.1029/2008GL037030.

Ardhuin, F., Rogers, W.E., Babanin, A.V., Filipot, J., Magne, R., Roland, A., van der Westhuysen, A., Queffeulou, P., Lefevre, J., Aouf, L. & Collard, F. (2010). Semiempirical dissipation source functions for ocean waves. Part I: Definition, calibration, and validation. *J. Phys. Oceanogr.* **40**, 1917–1941.

Aster, R.C., McNamara, D.E. & Bromirski, P.D. (2008). Multidecadal climate induced variability in microseisms. *Seismol. Res. Lett.* **79**, 194–202. doi:10.1785/gssrl.79.2.194

Barber, B.F. & Ursell, F. (1948). The generation and propagation of ocean waves and swell. I. Wave periods and velocities. *Phil. Trans. R. Soc. Lond. A*, **240**(824), 527–560.

Bauer, E. & Heimbach, P. (1999). Annual validation of significant wave heights from ERS-1 synthetic aperture radar wave mode spectra using TOPEX/POSEIDON and ERS-1 altimeter data. *J. Geophys. Res.* **104**(C6), 13 345–13 357. doi:10.1029/1999JC900014

Borge, J.C.N., Lehner, S. Niedermeier, A. & Schulz-Stellenfleth, J. (2004). Detection of ocean wave groupiness from spaceborne synthetic aperture radar. *J. Geophys. Res.* **109**, C07005. doi:10.1029/2004JC002298

Breivik, L.A., Reistad, M. Schyberg, H. Sunde, J. Krogstad, H.E. & Johnsen, H. (1998). Assimilation of ERS SAR wave spectra in an operational wave model. *J. Geophys. Res.*, **103**(C4), 7887–7900.

Brooker, G. (1995). *UWA Processing Algorithm Specification*, version 2.0, Tech. Rep., ESTEC/NWP, Noordwijk, The Netherlands.

Chapron, B., Collard, F. & Ardhuin, F. (2005). Direct measurements of ocean surface velocity from space: interpretation and validation, *J. Geophys. Res.* **110**, C07008. doi:10.1029/2004JC002809

Chapron, B., Johnsen, H. & Garello, R. (2001). Wave and wind retrieval from SAR images of the ocean. *Ann. Telecommun.* **56**, 682–699.

Collard, F., Ardhuin, F. & Chapron, B. (2005). Extraction of coastal ocean wave fields from SAR images. *IEEE J. Oceanic. Eng.* **30**(3), 526—533.

Collard, F., Ardhuin, F. & Chapron, B. (2009). Monitoring and analysis of ocean swell fields from space: New methods for routine observations. *J. Geophys. Res.* **114**, C07023. doi: 10.1029/2008JC005215

Delpey, M.T., Ardhuin, F. Collard, F. & Chapron, B. (2010). Space–time structure of long ocean swell fields. *J. Geophys. Res.* **115**, C12037. doi:10.1029/2009JC005885

Dysthe, K., Müller P. & Krogstad, H.E. (2008). Oceanic rogue waves. *Ann. Rev. Fluid Mech.* **40**, 287–310.

Ebeling, C. W., & Stein, S. (2011). Seismological Identication and characterization of a large hurricane. *Bull. Seismol. Soc. Am.* **101**(1), doi: 10.1785/0120100175

Engen G. & Johnsen, H. (1995). SAR-ocean wave inversion using image cross spectra. *IEEE Trans. Geosci. Rem. Sens.* **33**(4), 1047–1056.

Engen G., Johnsen H., Krogstad, H.E. & Barstow, S.F. (1994). Directional wave spectra by inversion of ERS-1 synthetic aperture radar ocean imagery. *IEEE Trans. Geosci. Rem. Sens.* **32**(2), 1994.

Grevemeyer, I., Herbert, R. & Essen, H.H. (2000). Microseismological eveidence for a changing wave climate in the northeast Atlantic Ocean. *Nature* **408**, 349–352.

Grob, M., Maggi, A. & Stutzmann, E. (2011). Observations of the seasonality of the Antarctic microseismic signal, and its association to sea ice variability. *Geophys. Res. Lett.*, **38**, L11302. doi: 10.1029/2011GL047525

Hanafin, J.A., Quilfen, Y., Ardhuin, F., Sienkiewicz, J., Queffeulou, P., Obrebski, M., Chapron, B., Reul, N., Collard, F., Corman, D., de Azevedo, E. B., Vandemark, D. & Stutzmann, E. (2012). Phenomenal sea states and swell from a North Atlantic storm in February 2011: A comprehensive analysis. *Bull. Am. Meteorol. Soc.* **93**(12), 1825–1832. doi: http://dx.doi.org/10.1175/BAMS-D-11-00128.1

Hasselmann, K. (1963). A statistical analysis of the generation of microseisms. *Rev. Geophys.* **1**, 177–210.

Hasselmann, K (1967). A criterion for nonlinear wave stability. *J. Fluid Mech.* **30**, 737–739.

Hasselmann, K. & Hasselmann, S. (1991). On the nonlinear mapping of an ocean wave spectrum into a Synthetic Aperture Radar image spectrum and its inversion. *J. Geophys. Res.* **96**, 10713–10729.

Hasselmann, K., Raney, R.K. Plant, W.J. et al. (1985). Theory of synthetic aperture radar ocean imaging: A MARSEN view. *J. Geophys. Res.* **90**, 4659–4686.

Hasselmann, S., Brüning, C. Hasselmann K. & Heimbach, P. (1996). An improved algorithm for the retrieval of ocean wave spectra from SAR image spectra. *J. Geophys. Res.* **C101**, 16615–16629.

Heimbach, P. & Hasselmann, K. (2000). Development and application of satellite retrievals of ocean wave spectra, In: D. Halpern (Ed.) *Satellites, Oceanograghy and Society*. Elsevier Oceanography Series vol. 63, Elsevier Science, Amsterdam, pp.5–33. doi:10.1016/S0422-9894(00)80003-3

Heimbach, P., Hasselmann, S. & Hasselmann, K. (1998). Statistical analysis and intercomparison with WAM model data of three years of global ERS-1 SAR wave mode spectral retrievals, *J. Geophys. Res.* **103**, 7931–7977.

Högström, U., Smedman, A., Sahleé, E., Drennan, W.M., Kahma, K.K., Pettersson, H. & Zhang, F. (2009). The atmospheric boundary layer during swell: a field study and interpretation of the turbulent kinetic energy budget for high wave ages. *J. Atmos. Sci.* **66**, 2764–2779. doi: http://dx.doi.org/10.1175/2009JAS2973.1

Holt, B., Liu, A.K. Wang, D.W., Gnanadesikan, A. & Chen, H.S. (1998). Tracking storm-generated waves in the northeast Pacific Ocean with ERS-1 synthetic aperture radar imagery and buoys. *J. Geophys. Res.* **103**(C4), 7917–7929.

Husson, R., Ardhuin, F., Collard, F., Chapron,B. & Balanche,A. (2012). Revealing forerunners on Envisat's wave mode ASAR using the Global Seismic Network. *Geophys. Res. Lett.*. **39**, L15609, doi: 10.1029/2012GL052334.

Janssen, P.A.E.M. (2003). Nonlinear four wave interaction and freak waves. *J. Phys. Oceanogr.* **33**, 863–884.

Janssen, P.A.E.M. (2008). Progress in ocean wave forecasting, *Comput. Phys.* **227**, 3572–3594.

Johannessen, J.A., Chapron, B., Collard, F., Kudryavtsev, V., Mouche, A., Akimov, D. & Dagestad, K.-F. (2008). Direct ocean surface velocity measurements from space: Improved quantitative interpretation of Envisat ASAR observations. *Geophys. Res. Lett.* **35**, L22608. doi:10.1029/2008GL035709

Johannessen, J.A., Chapron, B., Alpers, W., Collard, F., Cipollini, P., Liu, A., Horstmann, J., da Silva, J., Portabella, M., Robinson, I.S., Holt, B., Wackerman, C. & Vachon, P. (2013) Satellite oceanography from the ERS Synthetic Aperture Radar and Radar Altimeter: A brief review. This volume.

Johnsen, H., Engen, G. & Lauknes, I. (1998). The Envisat ASAR wave mode cross-spectra algorithm, Proc. *CEOS SAR Workshop*, February 1998, ESTEC/ESA.

Johnsen, H., Engen, G. Collard, F., Kerbaol, V. & Chapron, B. (2006). Envisat ASAR wave mode products: Quality assessment and algorithm upgrade. Proc. SEASAR 2006, Frascati, Italy. ESA SP-614, European Space Agency, Noordwijk, the Netherlands.

Kerbaol, V., Chapron, B. & Vachon, P.W. (1998) Analysis of ERS-1/2 synthetic aperture radar wave mode imagettes. *J. Geophys. Res.* **103**, 7833–7846.

Koenig, T., Lehner, S. & Schulz-Stellenfleth, J. (2007). Global analysis of a 2 year ERS-2 wave mode dataset over the Ocean, *Proc. IGARSS 2007*, Barcelona, Spain.

Komen, G.J., Cavaleri, L., Donelan, M., Hasselmann, K., Hasselmann, S. & Janssen, P.A.E.M. (1996). *Dynamics and Modelling of Ocean Waves*, Cambridge University Press, Cambridge, UK.

Krogstad, H. E. (1992). A simple derivation of Hasselmann's nonlinear ocean-SAR transformation. *J. Geophys. Res.* **97**(C2), 2421–2425.

Krogstad, H. E., Samset, O. & Vachon, P.W. (1994). Generalisations of the non-linear ocean–SAR transform O. and a simplified SAR inversion algorithm. *Atmos. Ocean* **32**(1), 61-82.

Lehner, S., (1984). *The Use of SAR for Large Scale Wind Measurement over the Ocean*. Hamburger geophysikalische Einzelschriften. M.L. Wittenborn Söhne, Hamburg.

Lehner, S., Schulz-Stellenfleth, J., Schättler, B., Breit, H. & Horstmann, J. (2000). Wind and wave measurements using complex ERS-2 wave mode data. *IEEE Trans. Geosci. Remote Sens.* **38**(5), 2246–2257.

Li, J.G & Holt, M. (2009). Comparison of ENVISAT ASAR ocean wave spectra with buoys and altimeter data via a wave model. *J. Atmos. Oceanic Technol.* **26**, 593–614.

Li, X.-M., Lehner, S. & Bruns, Th. (2011). Ocean wave integral parameter measurements using ENVISAT ASAR wave mode data, *IEEE Trans. Geosci. Rem. Sens.* **49**(1), 155–174. doi: 10.1109/TGRS.2010.2052364

Li, X.-M., König, Th., Schulz-Stellenfleth J. & Lehner, S. (2010). Validation and intercomparison of ocean wave spectra retrieval scheme using ASAR wave mode data. Int. *J. Remote Sens.* **31**(17), 4969–4933. DOI: 10.1080/01431161.2010.485222

Liu, A.K., Peng, C.Y. & Schumacher, J.D. (1994). Wave–current interaction study in the Gulf of Alaska for detection of eddies by synthetic aperture radar. *J. Geophys. Res.* **99**(C5), 10 075–10 085. doi: 10.1029/94JC00422

Longuet-Higgins, M. (1950) A theory of the origin of microseisms. *Phil. Trans. R. Soc. London, A*, **243**, 1–35.

Mastenbroek, C. & de Valk, C.F. (2000). A semi-parametric algorithm to retrieve ocean wave spectra from synthetic aperture radar. *J. Geophys. Res.* **105**, 3497–3516. doi:10.1029/1999JC900282

Niedermeier, A., Borge, J.C.N., Lehner, S. & Schultz-Stellenfleth, J. (2005). A wavelet-based algorithm to estimate ocean wave group parameters from radar images. *IEEE Trans. Geosci. Rem. Sens.* **43**(2), pp. 327–336. doi: 10.1109/TGRS.2004.836873

Schulz-Stellenfleth, J. & Lehner, S. (2004). Measurement of two-dimensional sea surface elevation fields using complex synthetic aperture radar data, *IEEE Trans. Geosci. Rem. Sens.* **42**, 1149–1160.

Schulz-Stellenfleth, J., Lehner S. & Hoja, D. (2005). A parametric scheme for the retrieval of two-dimensional ocean wave spectra from synthetic aperture radar look cross spectra. J. Geophys. Res, 110, C05004. doi: 10.1029/2004JC002822

Schulz-Stellenfleth, J., König, Th. & Lehner, S. (2007). An empirical approach for the retrieval of integral ocean wave parameters from synthetic aperture radar data. *J. Geophys. Res.* **112**, doi: 10.1029/2006JC003970

Snodgrass, F.E., Groves, G.W., Hasselmann, K., Miller, G.R., Munk, W.H. & Powers, W.H. (1966). Propagation of ocean swell across the Pacific. *Phil. Trans. R. Soc. London* **249A**, 431–497.

Tamura, H., Waseda, T. & Miyazawa, Y. (2010). Impact of nonlinear energy transfer on the wave field in Pacific hindcast experiments. *J. Geophys. Res.* **115**, C12036. doi: 10.1029/2009JC006014

Tamura, H., Waseda, T., Miyazawa, Y. & Komatsu, K. (2008). Current-induced modulation of the ocean wave spectrum and the role of nonlinear energy transfer. *J. Phys. Oceanogr.* **38**, 2662–2684.

Tolman, H.L. (2004). Inverse modeling of discrete interaction approximations for nonlinear interactions in waves. *Ocean Modelling* **6**, 405–422.

Tolman, H.L. (2009). Practical nonlinear interaction algorithms. *Proc. 11th Int. Workshop on Wave Hindcasting and Forecasting, and 2nd Coastal Hazards Symp.*, Halifax, Nova Scotia, Canada.

Tolman, H.L. (2011). On the impact of nonlinear interaction parameterizations in practical wave models. *Proc. 12th Int. Workshop on Wave Hindcasting and Forecasting, and 3rd Coastal Hazards Symp.*, Hawaii, USA.

Tolman, H.L., Banner, M. & Kaihatu, J. (2011). The NOPP Operational Wave Model Improvement Project, *Proc. 12th Int. Workshop on Wave Hindcasting and Forecasting, and 3rd Coastal Hazards Symp.*, Hawaii, USA.

Ueno, K. & Kohno, N. (2004). The development of the third generation model MRI-III for operational use, *Proc. 8th Int. Workshop on Wave Hindcasting and Forecasting* G2, pp.1–7.

Vachon, P.W. & West, J.C. (1992). Spectral estimation techniques for multilook SAR images of ocean waves. *IEEE Trans. Geosci. Rem. Sens.* **30**(3), 568–577.

Vachon, P.W. & Raney, R.K. (1991). Resolution of the ocean wave propagation direction in SAR imagery. *IEEE Trans. Geosci. Rem. Sens.* **29**(91), 105–112.

Van Vledder, G.P. (2001). Extension of the discrete interaction approximation for computing nonlinear quadruplet wave–wave interactions in operational wave models, *Proc. 4th ASCE Int. Symp. on Ocean Waves, Measurements and Analysis*, San Francisco, CA, USA, pp.540–549.

WAMDI Group (1998). The WAM model – a third generation ocean wave prediction model. *J. Phys. Oceanogr.* **18**, 1775–1810.